Genetic influences on the intrinsic and extrinsic functional organizations of the cerebral cortex

Running title: GWAS of cerebral cortex functions

Bingxin Zhao[1], Tengfei Li[2,3], Stephen M. Smith[4], Zirui Fan[1], Di Xiong[5], Xifeng Wang[5], Yue Yang[5], Tianyou Luo[5], Ziliang Zhu[5], Yue Shan[5], Yujue Li[1], Zhenyi Wu[1], Heping Zhang[6], Yun Li[5,7,8], Jason L. Stein[7,9], and Hongtu Zhu[3,5,7,8,10]*

[1]Department of Statistics, Purdue University, West Lafayette, IN 47907, USA.

[2]Department of Radiology, University of North Carolina at Chapel Hill, Chapel Hill, NC 27599, USA.

[3]Biomedical Research Imaging Center, School of Medicine, University of North Carolina at Chapel Hill, Chapel Hill, NC 27599, USA.

[4]Wellcome Centre for Integrative Neuroimaging, FMRIB, Nuffield Department of Clinical Neurosciences, University of Oxford, Oxford, UK.

[5]Department of Biostatistics, University of North Carolina at Chapel Hill, Chapel Hill, NC 27599, USA.

[6]Department of Biostatistics, Yale University, New Haven, CT 06511, USA.

[7]Department of Genetics, University of North Carolina at Chapel Hill, Chapel Hill, NC 27599, USA.

[8]Department of Computer Science, University of North Carolina at Chapel Hill, Chapel Hill, NC 27599, USA.

[9]UNC Neuroscience Center, University of North Carolina at Chapel Hill, Chapel Hill, NC 27599, USA.

[10] Department of Statistics and Operations Research, University of North Carolina at Chapel Hill, Chapel Hill, NC 27599, USA.

**Corresponding author*:

Hongtu Zhu

3105C McGavran-Greenberg Hall, 135 Dauer Drive, Chapel Hill, NC 27599.

E-mail address: htzhu@email.unc.edu Phone: (919) 966-7250

Abstract

The human cerebral cortex plays a crucial role in brain functions. However, genetic influences on the human cortical functional organizations are not well understood. Using a parcellation-based approach with resting-state and task-evoked functional magnetic resonance imaging (fMRI) from 40,253 individuals, we identified 47 loci associated with functional areas and networks at rest, 15 of which also affected the functional connectivity during task performance. Heritability and locus-specific genetic effects patterns were observed across different brain functional areas and networks. Specific functional areas and networks were identified to share genetic influences with cognition, mental health, and major brain disorders (such as Alzheimer's disease and schizophrenia). For example, in both resting and task fMRI, the *APOE* ε4 locus strongly associated with Alzheimer's disease was particularly associated with the visual cortex in the secondary visual and default mode networks. In summary, by analyzing biobank-scale fMRI data in high-resolution brain parcellation, this study advances our understanding of the genetic determinants of cerebral cortex function and prioritizes genetically associated fMRI traits for clinical applications of specific brain disorders.

Keywords: Brain disorders; Brain function; fMRI; GWAS; Mental health; UK Biobank.

The human cerebral cortex is the largest part of the human brain and controls complex brain functions. Based on known functional and topographic specializations at different scales, the cerebral cortex of the human brain can be divided into distinct areas and networks, providing insight into the brain's functional architecture[1,2]. To define such brain partitions, a few brain parcellations have been developed over the past decade[3]. In functional magnetic resonance imaging[4,5] (fMRI), cerebral cortex functions can be evaluated by measuring functional connectivity (or correlation of blood-oxygen-level dependent (BOLD) activity) among multiple cortical areas along a given parcellation. In particular, resting-state fMRI captures the intrinsic functional organization of the cortex without any explicit stimuli, whereas task-evoked fMRI measures extrinsic cortical interaction and temporal synchrony in response to a specific task. A variety of clinical applications of both task-evoked and resting-state fMRI have revealed changes in brain function in multiple neurological and psychiatric disorders, such as schizophrenia[6], Alzheimer's disease[7], Parkinson's disease[8], autism spectrum disorders[9], and major depressive disorder (MDD)[10].

Recently, growing literature suggested that fMRI measures may have lower test re-test reliability than imaging measures of brain structures[11,12]. As a result, large sample size is particularly important in fMRI studies to generate reproducible findings[12,13]. For example, fMRI images from thousands of individuals might be needed in association analysis with human behavioral traits[12]. Moreover, although twin studies have consistently established that brain resting and task fMRI traits are moderately heritable[14-21] (for example, heritability range of resting fMRI was (0.2,0.6) in a recent review[22]), large imaging genetic cohorts are required to identify the specific genetic variants associated with functional brain. Fortunately, a few big fMRI databases have become publicly available in recent years, including the Adolescent Brain Cognitive Development[23] (ABCD) and the UK Biobank[24] (UKB). Particularly, the UKB imaging study aimed to collect data from 100,000 subjects[25], providing new opportunity for fMRI research in one large-scale cohort. Using a whole brain spatial independent component analysis (ICA)[26-28] approach in the UKB study, the narrow sense single-nucleotide polymorphism (SNP) heritability of resting fMRI traits was reported to be around 10% across the entire brain and higher than 30% in some functional regions[29]. A few genome-wide association studies (GWAS)[29-31] have also been

recently conducted on resting fMRI using these whole brain ICA-based traits. The whole brain ICA is a parcellation-free dimension reduction method that estimates the functional brain regions (i.e., ICA components/regions) directly from the fMRI data. Although the whole brain ICA is a powerful and popular fMRI tool, it is a data-driven method, which might limit its generalizability and interpretability[32]. Specifically, the whole brain ICA attempts to capture major variations in the data. As a result, ICA regions typically have large sizes, limiting their ability to capture high-resolution details of brain functionality. For example, an earlier study[28] defined 55 ICA components in the UK Biobank[33] (UKB) dataset, most of which are distributed across multiple brain areas and networks[30]. It may be difficult for ICA to prioritize specific brain regions for specific brain disorders, limiting the use of fMRI phenotypes in clinical/translational research. Moreover, it might be difficult to use ICA to compare intrinsic and extrinsic functional architectures, since the ICA components estimated in resting and task fMRI may not be well-aligned.

To overcome these limitations, here we used a parcellation-based approach to provide fine-grained details about the genetic architecture of cerebral cortex functional organizations. A recently developed human brain parcellation[1], which partitioned the cerebral cortex into 360 areas (referred to as the Glasser360 atlas hereafter, **Table S1** and **Fig. 1A**), was used to analyze resting and task fMRI data of 40,253 individuals in the UKB study. The task implemented in the UKB fMRI study was an emotional processing task[34,35], known to robustly activate amygdala and visual systems. The Glasser360 atlas was constructed using high-quality multi-modality data from the Human Connectome Project (HCP[36]) and greatly improved the neuroanatomical resolution of human cerebral cortex annotations. The 360 cortical areas were grouped into 12 functional networks[37], including four well-known sensory networks (the primary visual, secondary visual, auditory, and somatomotor), four cognitive networks (the cingulo-opercular, default mode, dorsal attention, and frontoparietal), the language network, and three recently identified networks (the posterior multimodal, ventral multimodal, and orbito-affective) (**Fig. 1A**). In addition to pairwise functional connectivity among areas, we developed a parcellation-based dimension reduction procedure to generate network-level fMRI traits via a combined principal component analysis (PCA) and ICA methods[29] in a training-validation design (**Fig. S1**). Briefly, area-level functional connectivity pairs within each network and

between each pair of networks were summarized into network-specific traits to quantify the strength of functional connectivity within each network and two different networks (Methods). Genetic architectures were examined at both area- and network-levels for brain functions using these functional connectivity traits. Together, there were 8,531 area-level traits and 1,066 network-level traits for resting fMRI and 8,531 area-level traits and 919 network-level traits for task fMRI. The large number of traits 1) enabled the comparison between intrinsic and extrinsic functional architectures using both resting and task fMRI; and 2) uncovered much more and finer detail on the genetic influences on specific functional areas and networks and their genetic links with brain-related complex traits and disorders. Most of the ICA components used in previous resting fMRI GWAS[29-31] overlapped with multiple Glasser360 areas and networks (mean number of areas = 20.97, **Fig. 1B** and **Fig. S2**). Thus, the current parcellation-based study provided more details and actionable findings for future clinical research. For example, we found that the *APOE* ε4 locus was particularly associated with the functional connectivity of the visual cortex in the secondary visual and default mode networks, prioritizing fMRI biomarkers for practical applications in Alzheimer's disease research.

RESULTS

Heritability of human cerebral cortex functional connectivity at rest and during a task.

We examined the heritability pattern of functional connectivity traits across different functional areas and networks. Using the UKB individuals of white British ancestry (n = 34,641 for resting and 32,144 for task), SNP heritability was estimated via GCTA[38] for the 8,531 area-level within-network functional connectivity traits in both resting and task fMRI. The mean heritability (h^2) was 10.4% for resting and 6.6% for task fMRI. Overall, the SNP heritability of 97.9% (8,349/8,531, h^2 range = (2.4%, 27.0%)) functional connectivity traits in resting fMRI and 80.8% (6,894/8,531, h^2 range = (2.9%, 24.1%)) functional connectivity traits in task fMRI remained significant after adjusting for multiple comparisons using the Benjamini-Hochberg procedure to control the false discovery rate (FDR) at 0.05 level (**Table S2**). We also estimated the heritability of the 1,985 network-level traits (1,066 for resting and 919 for task), 1049 resting fMRI traits and 893 task fMRI traits were significant at the FDR 0.05 level. The mean h^2 was 32.2% for amplitude traits (h^2 range = (20.8%, 46.1%)) and 12.2% for functional connectivity traits in resting fMRI (h^2

range = (3.3%, 32.7%)); and that was 19.6% for amplitude traits (h^2 range = (11.3%, 23.7%)) and 10.6% for functional connectivity traits (h^2 range = (3.4%, 24.9%)) in task fMRI (**Table S3**). The higher heritability of network-level fMRI traits may suggest that our dimension reduction approach reduces noise by aggregating fMRI signals or that genetics have a stronger influence on broader brain networks rather than specific area pairs. In addition, the average heritability of Glasser360 parcellation-based traits was higher than that of the whole brain ICA-based traits[29-31] estimated from almost the same UKB resting fMRI dataset (mean = 9.3% and 27.5% for functional connectivity and amplitude traits, respectively). The results were summarized in **Figure S3**. Further, as illustrated below, the parcellation-based traits revealed more area- and network-specific information about genetic influences on the human brain.

Figure 2A and **Figure S4A** illustrate the heritability pattern across different networks. The mean heritability was highest in the ventral multimodal network in resting fMRI (mean = 20.4%). The ventral multimodal is a recently identified network, consisting of four cortical areas (left/right TF and PeEc) on the ventral surface of the temporal lobe[37]. One possible function of this network is to represent higher-order semantic categories[37]. In addition, the mean heritability of task fMRI was lower than that of resting fMRI in all networks except for the secondary visual network, where more than half (52.32%) of connectivity traits had greater heritability in task fMRI than in resting fMRI (**Fig. S4B**). This might be partly because the visual cortex is highly activated when performing the emotional processing task[34,35]. We also compared the estimates of genetic variance between the resting and task fMRI. The genetic variance was generally reduced in task fMRI ($P < 2.2 \times 10^{-16}$) and spatial patterns were similar to those of heritability (**Figs. S5-S6**). Overall, large-scale fMRI data indicate different genetic influences in resting and task functional connectivity measurements.

In each network, the heritability pattern across functional areas was identified. For example, according to physical locations, the areas of the default mode network can be divided into seven clusters (**Fig. S7**). There is no significant correlation between the physical distance of these default mode area pairs and their heritability measurements ($P = 0.563$). In the visual cluster (including the precuneus, calcarine, and cingulate) and the

temporal cluster, the default mode connectivity traits were most heritable. Additionally, the connectivity traits between the two clusters and the angular and frontal clusters showed high heritability, indicating the high degree of genetic control of functional interaction among these physically disconnected regions (**Fig. 2B**). In the somatomotor network, the left/right 3a, 3b, and 4 areas (in the postcentral, precentral, and paracentral) and the left/right 7AL and 7PC areas (in the superior parietal) form two separate connectivity clusters. We found that the 3a, 3b, and 4 areas had the highest heritability within the somatomotor network, while the heritability of the 7AL and 7PC areas was low. In addition, the connectivity traits associated with the left OP2-3 area (in the Rolandic operculum and insula) had high heritability (**Fig. S8**). In the cingulo-opercular network, the insula-related areas (e.g., the left/right FOP5, PoI1, FOP3, FOP1, FOP4, MI, and PoI2) exhibited the highest heritability. However, the heritability of the adjacent para-insular area (the left/right PI, in the temporal pole and superior temporal) was low (**Fig. S9**). The insula is a functionally diverse part of the cortex involved in multiple functions, including emotion, cognition, and sensory perception[39,40]. The insula has been found to have the highest heritability in surface curvature analysis of cortical morphometry[20]. Additionally, the connectivity traits of several specific areas showed consistently high heritability in resting fMRI, including the left/right IPS1 areas (in the superior occipital) of the secondary visual network and the right TE1m and left/right TE1p areas (in the inferior temporal and middle temporal) of the frontoparietal network (**Fig. S10**). In task fMRI, we also observed a few areas that had higher heritability than others, including the visual cluster, left OFC (orbitofrontal complex), and left/right 25 areas (in the olfactory cortex) of the default mode network (**Fig. S11**); the left/right RSC (in the middle cingulate), POS2 (in the precuneus and cuneus), 7Pm (in the precuneus) areas of the frontoparietal network (**Fig. S12**); and the middle cingulate-related areas (e.g., the left/right p24pr, a24pr, and left 33pr) of the cingulo-opercular network (**Fig. S13**). In summary, our results illustrate the variations of genetic influences in the cerebral cortex and underscore the important functional areas whose interactions are strongly influenced by genetic factors.

The heritability pattern was also correlated with the activation maps defined in task fMRI (Shapes activation, Faces activation, and Faces-Shapes contrast)[28]. In resting fMRI, the heritability of functional connectivity traits located in task-defined activated regions was

lower than that of nonactivated functional connectivity traits (**Fig. 2C**, mean = 8.9% vs. 10.8%, $P < 2.2 \times 10^{-16}$). However, in task fMRI, activated traits had higher heritability than nonactivated ones (mean = 7.4% vs. 6.3%, $P < 2.2 \times 10^{-16}$). Similar results were also observed on genetic variance estimates ($P < 2.2 \times 10^{-16}$, **Fig. S5B**). These differences can be partially explained by the task-related changes in brain functional activities and inter-regional connectivities[41]. Our findings may also be related to previous observations that the correlation between two activated regions increases during task performance, whereas the correlation between other regions is decreased[42]. Overall, these results provide insights into the genetic influences on the intrinsic and extrinsic functional architecture.

Genetic loci associated with cerebral cortex functional areas and networks

GWAS was performed for the 8,531 × 2 within-network area-level connectivity traits in resting and task fMRI using the UKB individuals of white British ancestry (Methods). The LDSC intercepts[43] were close to one, suggesting no genomic inflation of test statistics due to confounding factors (mean intercept = 1.0002, range = (0.987, 1.019)). At a stringent significance level 2.93×10^{-12} (5×10^{-8}/8,531/2, additionally adjusted for the number of traits studied), we identified independent (linkage disequilibrium [LD] $r^2 < 0.1$) significant associations in 32 genomic regions (cytogenetic bands) for resting fMRI, 9 of which were also associated with task fMRI (**Fig. 3A** and **Table S4**).

Enrichment of locus-specific genetic effects was observed across different areas and networks in resting fMRI. Many of the fMRI-associated genetic variants are known to affect gene expressions in previously published human brain expression quantitative trait loci (eQTL) datasets[44,45]. For example, most of the associations of the 2q14.1 locus were in the somatomotor network. The 2q14.1 locus was also particularly associated with the right MST and right V6 areas (in the middle temporal and cuneus) of the secondary visual network and a few areas (e.g., the left/right 43 in the Rolandic operculum and the p24pr in the middle cingulate) of the cingulo-opercular network (**Fig. S14**). **Figure S15** illustrates the genes presented at this locus and shows that the index variant (and its proxy variants, LD $r^2 > 0.8$) are associated with the expression of *PAX8* and *FOXD4L1* in brain tissues[44], suggesting that the two genes are relevant to neuronal function. The 10q23.33 and

10q26.3 loci were mainly associated with the cingulo-opercular, somatomotor, auditory, and default mode networks (**Figs. S16-S17**). The index variants were eQTLs of *NOC3L, PLCE1,* and *INPP5A* (**Fig. S18**). Moreover, most of the 10q26.3-associated areas of the default mode network were in the hippocampal cluster (**Fig. S19**). The 3p11.1 locus had genetic effects on a few specific areas, including right PSL (Perisylvian language area, in the superior temporal) and left PF (in the supramarginal) areas of the cingulo-opercular network and the left PGs (in the angular) and the left 31a areas (in the middle cingulate) of the default mode network (**Figs. S20-S21**). The 11q22.1 locus was associated with the auditory network (especially the left MBelt [medial belt complex] area) and the insula-related areas (e.g., the left/right PoI1, PoI2, FOP3, MI, FOP4) of the cingulo-opercular network (**Fig. S22**). The significant variants were eQTLs of *CFAP300* (**Fig. S23**). The 15q14 locus was mainly associated with areas of the somatomotor and cingulo-opercular networks, such as the left FOP2 (in the Rolandic operculum) and the left 6r (in the opercular part of the inferior frontal) (**Figs. S24-S25**).

Interesting, all associations at the 19q13.32 locus, which was the major genetic risk factor of the late onset Alzheimer's disease, were in the secondary visual network (such as the left LO1 and right V3CD in middle occipital, left/right V3A in superior occipital, and left/right V6 in cuneus), with one exception in the visual cluster of the default mode network (**Fig. 3B** and **Figs. S26-S27**). These results highlight the close relationship between the 19q13.32 locus and the functional connectivity measurements of the visual cortex. Similarly, the variants in 10q26.13 locus were particularly associated with the visual cluster of the default mode network and were eQTLs of *LHPP* and *EEF1AKMT2* (**Figs. S28-S29**). The 17p11.2 locus was mainly associated with the insula-related areas (e.g., the left/right MI and FPO4) and the middle cingulate-related areas (e.g., the left/right a24pr and p32pr) of the cingulo-opercular network (**Fig. S30**). The significant variants were eQTLs of *GRAPL* (**Fig. S31**). The variants in 3q24 locus were related to the cingulo-opercular and frontoparietal networks and were eQTLs of *ZIC4* (**Figs. S32-S33**). Additionally, we found that the 4q24 locus was mainly associated the left 6ma area (in the superior frontal) of the cingulo-opercular network, the 14q23.1 locus with the left IPS1 area (in the superior occipital) of the secondary visual network, and the 2p21 locus with the left i6-8 area (in the middle frontal) of the frontoparietal network (**Figs. S34-S39**).

Among the 9 significant genomic regions identified in task fMRI, the 10q23.33 locus was mainly associated with the visual cluster of the default mode network (**Figs. S40-S41**), especially the left/right 31pv areas (in the middle cingulate) (**Fig. S42**). For other loci (e.g., 10q26.3, 3p11.1, and 19q13.32), the associated networks were similar to those in resting fMRI, although the number of connectivity traits surviving the stringent significance level became much smaller. We examined the pairwise genetic correlations between the 8,531 connectivity traits in resting and task fMRI via the cross-trait LD score regression[46] (Methods). The average genetic correlation among all the 8,531 pairs was 0.554, 3,598 of which were significant at the FDR 5% level (**Fig. S43**, mean = 0.710, standard error = 0.192). Although it was more difficult to identify associated loci for task fMRI, these strong genetic correlations suggest the overall similarity of the genetic architecture on brain functions at rest and during a task.

Next, we performed GWAS for the 1,985 network-level traits to identify variants associated with network-specific functional connectivity measurements (within each of the 12 networks and between each pair of networks). At the 2.51×10^{-11} ($5 \times 10^{-8}/1{,}985$) significance level, we identified 41 (15 additional) genomic regions for resting fMRI, 14 of which were also associated with task fMRI (**Table S5**). On average, these 41 genetic regions explained 13.5% of the heritability of network-level fMRI traits. Together, the area- and network-level analysis identified 47 genomic regions for resting fMRI, 15 of which were also associated with task fMRI (**Fig. 3A**). The whole brain ICA analysis on largely the same resting fMRI dataset identified 45 associated genomic regions[30,31] ($P < 2.81 \times 10^{-11}$, $5 \times 10^{-8}/1{,}777$). Of the 45 regions, 31 were also identified in our study, with more detailed association patterns being uncovered (**Table S6** and **Fig. S44**). For example, the 19q13.32 region (index variant rs429358) had been found to be associated with the amplitude traits of large ICA-defined regions spanning multiple cognitive and visual networks. In the present study, as shown in **Figures 3B** and **S26-S27,** the area- and network-specific fMRI traits prioritized associations with the visual cortex. Furthermore, we identified 16 new loci that were associated with multiple areas and networks. For example, the 12p11.22 region (index variant rs11049367) was associated with the functional connectivity traits of the frontoparietal and default mode networks, especially

the connectivity between the right p9-46v and right TE1m areas in the frontoparietal network ($P < 2.12 \times 10^{-11}$). In addition, of the 47 fMRI-associated loci, 19 had been linked to brain structural connectivity traits in a recent study of white matter microstructure using diffusion MRI (dMRI)[47] (**Table S7**). A few of the 19 overlapped loci had wide genetic effects on multiple white matter tracts and functional networks, such as the 16q24.2, 3p11.1, 16q24.2, and 15q14 (**Fig. S45**).

Finally, we aimed to replicate the identified genomic loci using independent European and non-European datasets. First, we repeated GWAS on a European dataset with 4,882 subjects, including European individuals in the UKB phase 4 data (early 2021 release, removed the relatives of our discovery sample) and individuals of white but non-British ancestry in UKB phases 1 to 3 data. For the 266 independent (LD $r^2 < 0.1$) network-locus associations in resting fMRI, 60 (22.6%) passed the Bonferroni significance level (1.9×10^{-4}, 0.05/266) in this validation GWAS, and 190 (71.4%) were significant at nominal significance level (0.05). All of the 190 significant associations had concordant directions in the two GWAS (**Fig. S46A**). Of the 47 identified genomic loci, at least one association of 13 loci (27.7%) passed the Bonferroni significance level and 37 (78.7%) can be validated at 0.05 nominal significance level. For task fMRI, 33% (i.e., 19/57) network-locus associations passed the nominal significance level, all of which had the same effect signs in the two GWAS (**Fig. S46B**). The 17 associations were related to nine genomic loci, four of which were significant at the Bonferroni significance level, including the 10q23.33, 16q24.2, 10q26.3, and 19q13.32. Next, we performed GWAS on two UKB non-European validation datasets: the UKB Asian (UKBA, $n = 469$) and UKB Black (UKBBL, $n = 261$). Of the 47 genomic loci, 16 (3 also in task) were validated in UKBA and 10 (5 also in task) were significant in UKBBL at nominal significance level, none of them survived the Bonferroni significance level (**Tables S4-S5**). Particularly, the 15q14 locus can be consistently validated for both resting and task fMRI in UKBA and UKBBL ($P < 5.0 \times 10^{-3}$).

The shared genetic influences with complex brain traits and disorders.

To evaluate the shared genetic influences between brain functional organizations and complex brain traits and diseases, we conducted association lookups for independent (LD

$r^2 < 0.1$) significant variants (and variants in LD, $r^2 \geq 0.6$) detected in the UKB white British GWAS. In the NHGRI-EBI GWAS catalog[48], our results tagged variants reported for a wide range of complex traits and diseases, such as neurological disorders, neuropsychiatric disorders, mental health and psychological traits, migraine, cognitive traits, educational attainment, sleep, smoking/drinking, and anthropometric measurements (**Table S8**). The top five frequently tagged regions included 19q13.32 (the most frequently reported gene in prior literature was *APOE*), 2q14.1 (*PAX8*), 10q23.33 (*PLCE1*), 17q21.31 (*MAPT*), and 6q16.1 (*FHL5*), which covering 81.66% of all tagged trait-variant associations. To explore the detailed colocalization pattern across brain functional areas, we further took the index variants of colocalized traits/diseases and performed variant-specific association analysis for all the 64,620 functional connectivity traits (Methods). Below we highlighted colocalizations in a few genomic regions (**Table S9**). All these loci have been replicated at nominal significance level in our validation GWAS.

The rs429358 (19q13.32), one of the two variants in the *APOE* ε4 locus, is a well-known risk factor of Alzheimer's disease. In this locus, we observed the shared genetic influences with Alzheimer's disease in both resting and task fMRI (**Figs. 4A-B**). We further applied Bayesian colocalization analysis[49] to test colocalization between fMRI traits and Alzheimer's disease, which was defined as having a posterior probability of the shared causal variant hypothesis (PPH4) > 0.8[49,50]. Strong colocalizations between fMRI traits and Alzheimer's disease were identified (PPH4 > 0.946). Furthermore, in both resting and task fMRI, the secondary visual network had the strongest association with rs429358 (**Fig. 4C** and **Fig. S47A**). The allele associated with increased risk for Alzheimer's disease ("C") was associated with decreased functional connectivity in visual cortex (**Fig. S48**). Visual deficits were one of the first symptoms of Alzheimer's disease[51] and functional connectivity deficits in the visual cortex have been reported in Alzheimer's disease[52,53]. Decreased eigenvector centrality in visual cortex was associated with *APOE* ε4 carriership among normal elderly subjects[54]. In addition, the risk allele at rs429358 was associated with decreased default mode activity at the Bonferroni significance level in variant-specific analysis (3.86×10^{-7}, 0.05/64,620/2), with distinct patterns in resting and task fMRI (**Fig. S47B**). In resting fMRI, the associations were mainly in the visual cluster and the left/right 10d areas (in the superior frontal). Decreased default mode network connectivity in the

posterior cingulate cortex/precuneus, orbital and middle frontal cortex, and inferior parietal lobe in *APOE* ε4 carriers is consistently reported in various studies across adulthood (see Section 3.3.1 and Table 2 of Foo, et al. [22]). Regardless of *APOE* carrier status, results from previous studies are consistent in finding decreased functional connectivity in the default mode network in subjects with Alzheimer's disease and mild cognitive impairment, as summarized in Dennis and Thompson [55] and Badhwar, et al. [7]. For task fMRI, most of the significant rs429358 effects were on the interactions between the visual cluster and a few areas in the frontal cluster, including the left/right p32 (in the medial superior frontal), a24 (in the pregenual anterior cingulate cortex), and 8Ad (in the superior frontal) areas. The reduced deactivation of the default mode network during tasks has been consistently observed in different stages of Alzheimer's disease[56] and normal carriers of the *APOE* ε4[57]. Biologically, amyloid-β (Aβ) accumulation preferentially starts in several of the core regions of the default mode network, and the earliest Aβ accumulation is further associated with hypoconnectivity within the default mode network and between default mode network and the frontoparietal network[58]. Furthermore, we found the risk allele at rs429358 decreased the functional connectivity of middle temporal areas in the language network (e.g., the left/right TPOJ and STSdp) and the left IP0 area (in the middle occipital) of the dorsal attention network in task fMRI, but not in resting fMRI (**Fig. S49**). We also tested the association between rs429358 and MRI traits of other imaging modalities, including structural connectivity traits from dMRI[47] and regional brain volumes from structural MRI (sMRI)[59]. The fMRI traits had much stronger associations (smaller *P*-values) with rs429358 than these structural traits. Together, these results suggest the fMRI traits of brain functions, especially the ones from the visual cortex in the secondary visual and default mode networks, might be more directly related to the genetic pathways of *APOE* ε4 to Alzheimer's disease than brain morphology. These fMRI traits could be used as imaging biomarkers in etiologic study of Alzheimer's disease and drug development targeting *APOE* ε4.

In the 17p11.2 and 2p16.1 regions, we observed the shared genetic influences between the default mode network and multiple psychiatric disorders, including schizophrenia[60,61], autism spectrum disorder[62], MDD[63], and epilepsy[64]. For example, we tagged the rs4273100 (nearest gene *EPN2*, 17p11.2) and rs1518395 (*VRK2*, 2p16.1), which have been

implicated with schizophrenia (**Fig. S50**). Rs1518395 was also a risk variant for MDD and the rs2947349 (*VRK2*, 2p16.1) was associated with epilepsy. In resting fMRI, all three index variants exhibited the strongest associations with the default mode network, especially the frontal cluster (**Figs. S51-S52**). In addition, we observed the shared genetic influences with cognitive ability and education[65] in the 17p11.2 region (e.g., rs12602286, *EPN2*) and with psychological traits (e.g., neuroticism[66] and subjective well-being[67], rs2678897, *VRK2*) in the 2p16.1 region, which were also mainly related to the default mode network (**Fig. S53**). Strong pairwise colocalizations were observed between fMRI traits and multiple brain-related disorders and complex traits, including schizophrenia (17p11.2, PPH4 = 0.956), education (17p11.2, PPH4 = 0.870), math ability (17p11.2, PPH4 = 0.965), and neuroticism (2p16.1, PPH4 = 0.922).

In the 10q23.33 and 6q16.1 regions, our identified variants tagged those that have been implicated with migraine[68,69] (**Fig. S54**). For example, the index variant rs11187838 (*PLCE1*, 10q23.33, PPH4 = 0.849) affected multiple networks and had the strongest associations in the auditory and cingulo-opercular networks (**Fig. S55**). The index variant rs11759769 (*FHL5*, 6q16.1) was associated with the auditory, cingulo-opercular, and ventral multimodal networks in resting fMRI (**Fig. S56**). We also tagged risk variants of brain aneurysm[70] (rs11187838) and cerebral blood flow[71] (rs2971609, *FHL5*, 6q16.1). Migraine is a heterogeneous disorder and no neuroimaging biomarker has been well established in previous small sample fMRI studies[72]. Our results may help identify whether the risk variants of migraine predispose to migraine in particular brain areas or networks. Specifically, our findings suggest the genetic overlaps among migraine, cerebrovascular traits, and brain functions across multiple networks, especially the auditory and cingulo-opercular networks.

The shared genetic influences with cognitive ability[65], intelligence[73], and education[65] were observed in the 10q26.13, 5q15, and 3p11.1 regions (**Fig. S57**). The index variants of these cognitive traits were associated with a few specific functional areas in the temporal and parietal lobes. For example, in the 10q26.13 locus, our tagged variants associated with math ability, education[65], and cocaine dependence[74] (rs2629540, *FAM53B*). Rs2629540 variant was particularly associated with the precuneus-related areas in different

networks, such as the right PCV in the posterior multimodal network, the left/right 7Pm in the frontoparietal network, and the right 31pd in the default mode network (**Fig. S58**). The precuneus is involved in a variety of complex functions and responds to a wide variety of cognitive processes[75]. In the 5q15 region, we observed shared genetic effects with cognitive performance, math ability, and education[65] (rs114468556, *NR2F1*), most of which were related to the left/right TPOJ2 areas (in the middle temporal) of the posterior multimodal network (**Fig. S59A**). The *NR2F1* is well studied in the arealization of the cerebral cortex[76]. Strong colocalizations were identified for Alzheimer's disease in both 10q26.13 and 5q15 regions (PPH4 > 0.880). In the 3p11.1, we tagged variants associated with intelligence[73] (rs7652296, *EPHA3*, PPH4 =0.923). The *EPHA3* is involved in axon guidance[77] and the rs7652296 was mainly associated with between-network connectivity of a few temporal and parietal areas, such as the right PSL (Perisylvian language area, in the superior temporal) and the left PF (in the supramarginal) of the cingulo-opercular network; the left PHT (in the middle temporal) of the dorsal attention network; the right PFm (in the inferior parietal) and the left TE1p (in the inferior temporal and middle temporal) of the frontoparietal network; the left PSL (in the superior temporal) and the right STSdp (in the middle temporal) of the language network; and the left PGs (in the angular) of the default mode network (**Fig. S59B**). These findings partially support the parieto-frontal integration theory of intelligence[78,79], uncovering the genetic overlaps between cognitive functions and specific temporal and parietal functional areas.

In addition, we found colocalized genetic effects with psychological traits (e.g., risk-taking behaviors[80]) in the 3q24 (rs2279829, *ZIC4*) and 3p12.1 (rs6762267, *CADM2*) regions (**Fig. S60**). Rs2279829 and rs6762267 were mainly related to the interactions among the frontoparietal, cingulo-opercular, and default mode networks, with the strongest genetic effects being on a few frontal areas (e.g., the left/right i6-8, left/right p9-46v, left a10p, right p24, right PEF). Increasing evidence suggests the frontal lobe plays an important role in risk-taking and risk behaviors[81] (**Fig. S61**). In summary, brain functions measured in fMRI has substantial area-specific genetic overlaps with complex brain traits and clinical outcomes. Uncovering the detailed genetic colocalized patterns may help understand how alterations in specific brain functions lead to risk for brain conditions and disorders.

Genetic correlations with complex traits.

To further explore the genetic links, we examined the genetic correlations (GC)[46] between fMRI traits and 50 complex traits, most of which were colocalized traits in the above association lookups, as well as additionally mental health traits and major brain disorders. First, we examined the genetic correlations with 4 global functional connectivity and amplitude traits (2 trait for resting and 2 for task). At the FDR 5% level (4 × 50 tests), we found the global fMRI traits were significantly associated with hypertension, neuroticism (e.g., feeling nervous and worry), sleep traits, and task-taking behaviors (e.g., automobile speeding) (**Table S10**). For example, resting functional connectivity was negatively correlated with neuroticism (feeling nervous, GC = -0.181, $P < 1.14 \times 10^{-4}$) and sleep duration (GC = -0.173, $P < 1.58 \times 10^{-4}$). Hypertension was negatively correlated with the global amplitude in task fMRI (GC = -0.282, $P < 7.34 \times 10^{-6}$).

Next, we explored the spatial patterns of genetic overlaps by evaluating the genetic correlations between complex traits and 8,531 functional connectivity traits. Area- and network-specific genetic overlaps were widely observed in resting fMRI. For example, at the FDR 5% level (8,531 tests), cognitive function had genetic correlations with cognitive networks (the cingulo-opercular, default mode, frontoparietal, and dorsal attention), such as the right IFSa area (in the triangular part of inferior frontal) (**Fig. 5A**). Most of the significant genetic correlations were negative, which suggest genetic effects predispose to less resting connectivity is associated with increased intelligence. For schizophrenia and cross-disorder[82], we found consistent positive genetic correlations with the default mode network (e.g., the left/right 47s in the posterior orbital and the left/right 8BL in the medial superior frontal) and negative genetic correlations with the secondary visual network (e.g., the left/right LIPv in the superior parietal) (**Figs. 5B** and **S62**). Similarly, we found neuroticism (feeling nervous) had positive genetic correlations with the default mode network (e.g., the right PGi in the angular) and negative genetic correlations with the secondary visual network (e.g., the right FST in the middle temporal and the right VMV3 in the fusiform) (**Fig. S63**).

Task fMRI provided additional insights into the genetic correlations with cognitive function (**Fig. 5C**). Like resting fMRI, the default mode network had negative genetic

correlations with cognitive function. The correlations were enriched in the connectivity measurements between the visual cluster and the frontal cluster (**Fig. S64A**). Moreover, the secondary visual and somatomotor networks (e.g., the right V6 in the cuneus, the left VMV2 in the lingual, the left VIP in the superior parietal, and the right OP2-3 in in Rolandic operculum and insula) had positive genetic correlations with cognitive function (**Fig. S64B**). In summary, these results show the default mode network has negative genetic correlations with cognition and positive genetic correlations with brain disorders and neuroticism. The genetic correlations with cognition had opposite directions in the default mode network and the secondary visual network in task fMRI, pointing to genetic influences on task specific brain activity. Patterns of other complex traits (e.g., snoring, sleep duration, hypertension, general risk tolerance, and education) were summarized in the **Supplementary Note** and **Figures S65-S66**. In summary, discovering genetic co-variations with complex traits and diseases in specific brain areas and networks might improve our understanding of how the brain function is affected by genetic risk factors and aid early detection and timely treatment of brain diseases.

Gene-level analysis and biological annotations.

Using GWAS summary statistics of network-level fMRI traits, MAGMA[83] detected 67 significant genes with 352 associations ($P < 1.34 \times 10^{-9}$, adjusted for 1,985 phenotypes). The area-level traits additionally yielded 7 associated genes for resting fMRI and 1 for task fMRI ($P < 1.55 \times 10^{-10}$, adjusted for 8,531 × 2 phenotypes, **Table 11**). Among the 75 genes, 30 had not been identified by the whole brain ICA analysis[30] (**Fig. S67**). We performed some functional lookups for these fMRI-associated genes. First, nine genes (*SSH2, CADM2, FAT3, ANO1, CSMD3, HELLS, CTR9, KANSL1,* and *ETV1*) had a high probability of being loss-of-function (LoF) intolerant[84] (pLI > 0.98), indicating its extremely intolerant of LoF variation. Second, 24 (*UFL1, MEF2C, CPED1, TBC1D12, KANSL1, CRHR1, RNF112, TBC1D5, ANKRD32, DGKB, HSPG2, ZIC1, GRAP, MFAP4, FADD, NOC3L, CADM2, LRRC37A, EFCAB5, PLCB1, FAM53B, METTL10, ARL17B,* and *STH*) of the 67 genes were also identified by a recent eQTL study of developing human brain[85]. Moreover, in the constructed transcriptional networks[86], *FAT3, MEF2C, CRHR1, NR2F1* and *VRK2* were within the *adult neurons, synaptic transmission, and neuron projection development* function module; *SSH2*, *HSPG2*, and *KANSL1* were within the *superficial layer neurons and splicing* module;

and *CADM2, PIP5K1B, ZIC1, CXXC4, ANKRD32, CSMD3 and GNA12* were within *developing neurons and axon guidance* module. These results indicate these genes have potential functions in biological processes of brain development and healthy aging. In addition, we applied FUMA[87] to map significant variants ($P < 2.51 \times 10^{-11}$) to genes via physical position, eQTL association, and 3D chromatin (Hi-C) interaction. FUMA yielded 226 associated genes, 166 of which were not discovered in MAGMA (**Table S12**). In addition, 5 of the fMRI-associated genes (*CALY*, *SLC47A1, SLC6A4, CYP2C8,* and *CYP2C9*) were targets for 51 nervous system drugs[88] (anatomical therapeutic chemical (ATC) code starts with "N"), which was a higher probability of overlap than by chance (P = 0.027, Methods). Specifically, there were 29 anti-depressants (N06A) to treat major depression disorder and related conditions, 13 anti-psychotics drugs (N05A) to manage psychosis, 4 psychostimulants (N06B) for ADHD and nootropics, and 2 anti-migraine (N02C) (**Table S13**).

To identify brain cell types where genetic variation leads to changes in brain function, we performed partitioned heritability analyses[89] for cell type specific regulatory elements. Specifically, we estimated partitioned heritability enrichment within differentially accessible chromatin of neurons (NeuN+, including two subtypes GABAergic [NeuN+/Sox6+] and glutamatergic neurons [NeuN+/Sox6-]) and glial cells (NeuN-, including oligodendrocyte [NeuN-/Sox10+], microglia and astrocyte [NeuN-/Sox10-])[90]. To identify global enrichment across the whole brain, we performed partitioned heritability using global functional connectivity and amplitude traits in resting fMRI. For both functional connectivity and amplitude traits, there was a much stronger enrichment in neuronal regulatory elements than in glia (**Fig. 6A**). For further resolution across brain networks, we also performed enrichment analysis for the mean amplitude of the 12 networks. In most functional networks, neurons were more enriched than glia, and the strongest neuronal enrichment was found in the posterior multimodal network (**Fig. 6B**). These findings may indicate that common variants associated with brain functional activity primarily affect the function of regulatory elements in neurons, which are expected to influence brain functional interactions.

DISCUSSION

Most previous large-scale genetic studies of brain imaging data have focused on brain structures. Nevertheless, brain functional traits could also connect genetic variations to mechanisms underlying behavioral differences[91]. Using resting and task fMRI data from the UK Biobank, we provided fine details of genetic influences on cerebral cortex functional architectures through a parcellation-based approach. We showed the similarities and differences of the genetic architecture of intrinsic and extrinsic functional organizations in heritability analysis, association analysis, and genetic links with cognition and disease. Genetic colocalization and correlation analyses uncovered important brain functional areas and networks that were genetically implicated in specific diseases and traits. Our results may help guide future clinical research and applications in the field of neurodegenerative and neuropsychiatric disorders. For example, structural MRI traits[92] (such as gray matter volumes) are frequently used as imaging biomarkers in practical applications of Alzheimer's disease. However, we found substantial genetic links between the visual cortex function and Alzheimer's disease, and there were stronger associations with *APOE* ε4 in fMRI traits than in structural MRI traits. These funding suggest that fMRI traits of the visual cortex may be used as endophenotypes of Alzheimer's disease.

At group mean level, prior literature has demonstrated that the intrinsic and extrinsic functional architectures are highly similar with small but consistent differences[41,93-96]. These task-related changes are essential for the human brain to adaptively alter its functionality via rapid changes in inter-regional functional connectivity[41]. Using large-scale individual level data in the UK Biobank, we showed the overall genetic similarity between resting and task fMRI (e.g., mean genetic correlation = 0.7). Although the genetic differences between resting and task fMRI are small, several lines of evidence suggest such differences could be important and are genetically related to cognition and brain diseases. For example, cognitive function had genetic correlations with the secondary visual and somatomotor networks during task performance, but not at rest.

Although many efforts have been made to understand the functional organizations of the human brain, there is no one widely-accepted standard pipeline for functional connectivity analysis in fMRI[97]. Our study is one of the first attempts to study the genetic architecture of brain functions using a parcellation-based approach in biobank-scale

dataset. The major difference between the whole brain ICA and parcellation-based approaches is that the ICA regions were large and typically distributed across multiple regions and different networks by combining their major variations. Compared to the recent whole brain ICA-based studies[29,31], our parcellation-based approach was able to uncover high-resolution fine details on the genetic effect patterns and enable the comparison between intrinsic and extrinsic functional architectures. More importantly, our results suggest the usefulness of specific fMRI phenotypes for different brain disorders from a genetic perspective.

There are a few limitations in the present study. First, the UKB participants were mostly middle-aged to elderly Europeans. Although we have illustrated the overall consistency of group mean maps between the HCP and UKB cohorts, nonlinear aging effects on brain functional connectivity have been widely observed[98]. It is of great interest to study the gene-age interactions and evaluate the generalizability of UKB results across the lifespan[99]. It is also interesting to investigate the population-specific genetic components when more large-scale fMRI data from global populations become available. Due to potentially different environmental influences and population-specific genetic effects, fMRI traits could have different heritability across ancestry groups. Second, the UKB task fMRI data were from a single emotion processing task[34,35]. Although previous studies have shown that the functional architectures of different tasks were highly similar[41,93,95], multi-task fMRI data may provide new insights in genetic studies. It might be possible to impute/predict multi-task fMRI data for UKB using the multi-task HCP data as training reference panels. To allow comparison between resting and task fMRI, our study focused on functional connectivity traits. It is also of great interest to study the genetics influences on task activation measures/maps for task fMRI. Finally, this study partitioned the cerebral cortex using the Glasser360 atlas. By applying other brain parcellations[3] to the large-scale UKB dataset, it will be possible to establish more useful imaging phenotypes for specific brain disorders.

METHODS

Methods are available in the ***Methods*** section.

Note: One supplementary information pdf file, one supplementary figure pdf file, and one supplementary table zip file are available.

ACKNOWLEDGEMENTS

This research was partially supported by U.S. NIH grants MH086633 (HT.Z.) and MH116527 (TF.L. and HP.Z.). We thank the individuals represented in the UK Biobank and HCP studies for their participation and the research teams for their work in collecting, processing and disseminating these datasets for analysis. We thank Doug Crabill for helpful conversations on computing. We would like to thank the University of North Carolina at Chapel Hill and Purdue University and their Research Computing group for providing computational resources and support that have contributed to these research results. We gratefully acknowledge all the studies and databases that made GWAS summary data available. This research has been conducted using the UK Biobank resource (application number 22783), subject to a data transfer agreement. HCP data were provided by the Human Connectome Project, WU-Minn Consortium (Principal Investigators: David Van Essen and Kamil Ugurbil; 1U54MH091657) funded by the 16 NIH Institutes and Centers that support the NIH Blueprint for Neuroscience Research; and by the McDonnell Center for Systems Neuroscience at Washington University.

AUTHOR CONTRIBUTIONS

B.Z., HT.Z., J.L.S., and S.M.S. designed the study. B.Z., TF.L., Y.Y., D.X., X.W., Z.Z., TY. L, Z.W., and Z.F. analyzed the data. TF. L., Z.Z., and Y.S. downloaded the datasets, processed fMRI data, and undertook quantity controls. Y.L. and HP.Z. provided feedback on study design and results interpretation. B.Z. wrote the manuscript with feedback from all authors.

CORRESPINDENCE AND REQUESTS FOR MATERIALS should be addressed to HT.Z.

COMPETETING FINANCIAL INTERESTS

The authors declare no competing financial interests.

REFERENCES

1. Glasser, M.F. *et al.* A multi-modal parcellation of human cerebral cortex. *Nature* **536**, 171-178 (2016).
2. Van Essen, D.C., Glasser, M.F., Dierker, D.L., Harwell, J. & Coalson, T. Parcellations and hemispheric asymmetries of human cerebral cortex analyzed on surface-based atlases. *Cerebral cortex* **22**, 2241-2262 (2012).
3. Eickhoff, S.B., Yeo, B.T. & Genon, S. Imaging-based parcellations of the human brain. *Nature Reviews Neuroscience* **19**, 672-686 (2018).
4. Biswal, B., Zerrin Yetkin, F., Haughton, V.M. & Hyde, J.S. Functional connectivity in the motor cortex of resting human brain using echo-planar MRI. *Magnetic resonance in medicine* **34**, 537-541 (1995).
5. Belliveau, J. *et al.* Functional mapping of the human visual cortex by magnetic resonance imaging. *Science* **254**, 716-719 (1991).
6. Mwansisya, T.E. *et al.* Task and resting-state fMRI studies in first-episode schizophrenia: A systematic review. *Schizophrenia research* **189**, 9-18 (2017).
7. Badhwar, A. *et al.* Resting-state network dysfunction in Alzheimer's disease: a systematic review and meta-analysis. *Alzheimer's & Dementia: Diagnosis, Assessment & Disease Monitoring* **8**, 73-85 (2017).
8. Wolters, A.F. *et al.* Resting-state fMRI in Parkinson's disease patients with cognitive impairment: A meta-analysis. *Parkinsonism & Related Disorders* **62**, 16-27 (2019).
9. Philip, R.C. *et al.* A systematic review and meta-analysis of the fMRI investigation of autism spectrum disorders. *Neuroscience & Biobehavioral Reviews* **36**, 901-942 (2012).
10. Mulders, P.C., van Eijndhoven, P.F., Schene, A.H., Beckmann, C.F. & Tendolkar, I. Resting-state functional connectivity in major depressive disorder: a review. *Neuroscience & Biobehavioral Reviews* **56**, 330-344 (2015).
11. Elliott, M.L. *et al.* What is the test-retest reliability of common task-functional MRI measures? New empirical evidence and a meta-analysis. *Psychological Science* **31**, 792-806 (2020).
12. Marek, S. *et al.* Towards reproducible brain-wide association studies. *BioRxiv* (2020).

13. Smith, S.M. & Nichols, T.E. Statistical challenges in “big data” human neuroimaging. *Neuron* **97**, 263-268 (2018).
14. Elliott, M.L. *et al.* General functional connectivity: Shared features of resting-state and task fMRI drive reliable and heritable individual differences in functional brain networks. *NeuroImage* **189**, 516-532 (2019).
15. Ge, T., Holmes, A.J., Buckner, R.L., Smoller, J.W. & Sabuncu, M.R. Heritability analysis with repeat measurements and its application to resting-state functional connectivity. *Proceedings of the National Academy of Sciences* **114**, 5521-5526 (2017).
16. Yang, Z. *et al.* Genetic and environmental contributions to functional connectivity architecture of the human brain. *Cerebral cortex* **26**, 2341-2352 (2016).
17. Miranda-Dominguez, O. *et al.* Heritability of the human connectome: A connectotyping study. *Network Neuroscience* **2**, 175-199 (2018).
18. Adhikari, B.M. *et al.* Heritability estimates on resting state fMRI data using ENIGMA analysis pipeline. (2018).
19. Blokland, G.A. *et al.* Quantifying the heritability of task-related brain activation and performance during the N-back working memory task: a twin fMRI study. *Biological psychology* **79**, 70-79 (2008).
20. Colclough, G.L. *et al.* The heritability of multi-modal connectivity in human brain activity. *Elife* **6**, e20178 (2017).
21. Teeuw, J. *et al.* Genetic and environmental influences on functional connectivity within and between canonical cortical resting-state networks throughout adolescent development in boys and girls. *Neuroimage* **202**, 116073 (2019).
22. Foo, H. *et al.* Genetic influence on ageing-related changes in resting-state brain functional networks in healthy adults: a systematic review. *Neuroscience & Biobehavioral Reviews* (2020).
23. Chaarani, B. *et al.* Baseline brain function in the preadolescents of the ABCD Study. *Nature Neuroscience*, 1-11 (2021).
24. Miller, K.L. *et al.* Multimodal population brain imaging in the UK Biobank prospective epidemiological study. *Nature Neuroscience* **19**, 1523-1536 (2016).

25. Littlejohns, T.J. *et al.* The UK Biobank imaging enhancement of 100,000 participants: rationale, data collection, management and future directions. *Nature communications* **11**, 1-12 (2020).
26. Beckmann, C.F. & Smith, S.M. Probabilistic independent component analysis for functional magnetic resonance imaging. *IEEE transactions on medical imaging* **23**, 137-152 (2004).
27. Hyvarinen, A. Fast and robust fixed-point algorithms for independent component analysis. *IEEE transactions on Neural Networks* **10**, 626-634 (1999).
28. Alfaro-Almagro, F. *et al.* Image processing and Quality Control for the first 10,000 brain imaging datasets from UK Biobank. *NeuroImage* **166**, 400-424 (2018).
29. Elliott, L.T. *et al.* Genome-wide association studies of brain imaging phenotypes in UK Biobank. *Nature* **562**, 210-216 (2018).
30. Zhao, B. *et al.* Common variants contribute to intrinsic human brain functional networks. *bioRxiv* (2020).
31. Smith, S.M. *et al.* An expanded set of genome-wide association studies of brain imaging phenotypes in UK Biobank. *Nature neuroscience* **24**, 737-745 (2021).
32. Lv, H. *et al.* Resting-state functional MRI: everything that nonexperts have always wanted to know. *American Journal of Neuroradiology* **39**, 1390-1399 (2018).
33. Sudlow, C. *et al.* UK biobank: an open access resource for identifying the causes of a wide range of complex diseases of middle and old age. *PLoS Medicine* **12**, e1001779 (2015).
34. Hariri, A.R., Tessitore, A., Mattay, V.S., Fera, F. & Weinberger, D.R. The amygdala response to emotional stimuli: a comparison of faces and scenes. *Neuroimage* **17**, 317-323 (2002).
35. Barch, D.M. *et al.* Function in the human connectome: task-fMRI and individual differences in behavior. *Neuroimage* **80**, 169-189 (2013).
36. Somerville, L.H. *et al.* The Lifespan Human Connectome Project in Development: A large-scale study of brain connectivity development in 5–21 year olds. *NeuroImage* **183**, 456-468 (2018).
37. Ji, J.L. *et al.* Mapping the human brain's cortical-subcortical functional network organization. *Neuroimage* **185**, 35-57 (2019).

38. Yang, J., Lee, S.H., Goddard, M.E. & Visscher, P.M. GCTA: a tool for genome-wide complex trait analysis. *The American Journal of Human Genetics* **88**, 76-82 (2011).
39. Türe, U., Yaşargil, D.C., Al-Mefty, O. & Yaşargil, M.G. Topographic anatomy of the insular region. *Journal of neurosurgery* **90**, 720-733 (1999).
40. Nieuwenhuys, R. The insular cortex: a review. *Progress in brain research* **195**, 123-163 (2012).
41. Cole, M.W., Ito, T., Cocuzza, C. & Sanchez-Romero, R. The functional relevance of task-state functional connectivity. *Journal of Neuroscience* **41**, 2684-2702 (2021).
42. Fox, M.D. & Raichle, M.E. Spontaneous fluctuations in brain activity observed with functional magnetic resonance imaging. *Nature reviews neuroscience* **8**, 700-711 (2007).
43. Bulik-Sullivan, B.K. *et al.* LD Score regression distinguishes confounding from polygenicity in genome-wide association studies. *Nature genetics* **47**, 291-295 (2015).
44. de Klein, N. *et al.* Brain expression quantitative trait locus and network analysis reveals downstream effects and putative drivers for brain-related diseases. *bioRxiv* (2021).
45. Hormozdiari, F. *et al.* Colocalization of GWAS and eQTL signals detects target genes. *The American Journal of Human Genetics* **99**, 1245-1260 (2016).
46. Bulik-Sullivan, B. *et al.* An atlas of genetic correlations across human diseases and traits. *Nature Genetics* **47**, 1236-1241 (2015).
47. Zhao, B. *et al.* Common genetic variation influencing human white matter microstructure. *bioRxiv* (2020).
48. Buniello, A. *et al.* The NHGRI-EBI GWAS Catalog of published genome-wide association studies, targeted arrays and summary statistics 2019. *Nucleic Acids Research* **47**, D1005-D1012 (2018).
49. Giambartolomei, C. *et al.* Bayesian test for colocalisation between pairs of genetic association studies using summary statistics. *PLoS genetics* **10**, e1004383 (2014).
50. Kibinge, N.K., Relton, C.L., Gaunt, T.R. & Richardson, T.G. Characterizing the causal pathway for genetic variants associated with neurological phenotypes

using human brain-derived proteome data. *The American Journal of Human Genetics* **106**, 885-892 (2020).

51. Brewer, A.A. & Barton, B. Visual cortex in aging and Alzheimer's disease: changes in visual field maps and population receptive fields. *Frontiers in psychology* **5**, 74 (2014).

52. Zhang, H.-Y. *et al.* Resting brain connectivity: changes during the progress of Alzheimer disease. *Radiology* **256**, 598-606 (2010).

53. Wang, Z. *et al.* Functional connectivity changes across the spectrum of subjective cognitive decline, amnestic mild cognitive impairment and Alzheimer's disease. *Frontiers in neuroinformatics* **13**, 26 (2019).

54. Wink, A.M. *et al.* Functional brain network centrality is related to APOE genotype in cognitively normal elderly. *Brain and behavior* **8**, e01080 (2018).

55. Dennis, E.L. & Thompson, P.M. Functional brain connectivity using fMRI in aging and Alzheimer's disease. *Neuropsychology review* **24**, 49-62 (2014).

56. Palop, J.J. & Mucke, L. Network abnormalities and interneuron dysfunction in Alzheimer disease. *Nature Reviews Neuroscience* **17**, 777-792 (2016).

57. Filippini, N. *et al.* Distinct patterns of brain activity in young carriers of the APOE-ε4 allele. *Proceedings of the National Academy of Sciences* **106**, 7209-7214 (2009).

58. Palmqvist, S. *et al.* Earliest accumulation of β-amyloid occurs within the default-mode network and concurrently affects brain connectivity. *Nature communications* **8**, 1-13 (2017).

59. Zhao, B. *et al.* Genome-wide association analysis of 19,629 individuals identifies variants influencing regional brain volumes and refines their genetic co-architecture with cognitive and mental health traits. *Nature genetics* **51**, 1637-1644 (2019).

60. Goes, F.S. *et al.* Genome-wide association study of schizophrenia in Ashkenazi Jews. *American Journal of Medical Genetics Part B: Neuropsychiatric Genetics* **168**, 649-659 (2015).

61. Li, Z. *et al.* Genome-wide association analysis identifies 30 new susceptibility loci for schizophrenia. *Nature Genetics* **49**, 1576-1583 (2017).

62. Anney, R.J.L. *et al.* Meta-analysis of GWAS of over 16,000 individuals with autism spectrum disorder highlights a novel locus at 10q24.32 and a significant overlap with schizophrenia. *Molecular Autism* **8**, 21 (2017).
63. Hyde, C.L. *et al.* Identification of 15 genetic loci associated with risk of major depression in individuals of European descent. *Nature genetics* **48**, 1031-1036 (2016).
64. Anney, R. *et al.* Genetic determinants of common epilepsies: a meta-analysis of genome-wide association studies. *The Lancet Neurology* **13**, 893-903 (2014).
65. Lee, J.J. *et al.* Gene discovery and polygenic prediction from a genome-wide association study of educational attainment in 1.1 million individuals. *Nature Genetics* **50**, 1112–1121 (2018).
66. Kichaev, G. *et al.* Leveraging polygenic functional enrichment to improve GWAS power. *The American Journal of Human Genetics* **104**, 65-75 (2019).
67. Baselmans, B.M. *et al.* Multivariate genome-wide analyses of the well-being spectrum. *Nature genetics* **51**, 445-451 (2019).
68. Pickrell, J.K. *et al.* Detection and interpretation of shared genetic influences on 42 human traits. *Nature genetics* **48**, 709 (2016).
69. Anttila, V. *et al.* Genome-wide meta-analysis identifies new susceptibility loci for migraine. *Nature genetics* **45**, 912 (2013).
70. Bakker, M.K. *et al.* Genome-wide association study of intracranial aneurysms identifies 17 risk loci and genetic overlap with clinical risk factors. *Nature genetics* **52**, 1303-1313 (2020).
71. Ikram, M.A. *et al.* Heritability and genome-wide associations studies of cerebral blood flow in the general population. *Journal of Cerebral Blood Flow & Metabolism* **38**, 1598-1608 (2018).
72. Skorobogatykh, K. *et al.* Functional connectivity studies in migraine: what have we learned? *The journal of headache and pain* **20**, 1-10 (2019).
73. Savage, J.E. *et al.* Genome-wide association meta-analysis in 269,867 individuals identifies new genetic and functional links to intelligence. *Nature Genetics* **50**, 912-919 (2018).

74. Gelernter, J. *et al.* Genome-wide association study of cocaine dependence and related traits: FAM53B identified as a risk gene. *Molecular psychiatry* **19**, 717-723 (2014).
75. Cavanna, A.E. & Trimble, M.R. The precuneus: a review of its functional anatomy and behavioural correlates. *Brain* **129**, 564-583 (2006).
76. Cadwell, C.R., Bhaduri, A., Mostajo-Radji, M.A., Keefe, M.G. & Nowakowski, T.J. Development and arealization of the cerebral cortex. *Neuron* **103**, 980-1004 (2019).
77. Nishikimi, M., Oishi, K., Tabata, H., Torii, K. & Nakajima, K. Segregation and pathfinding of callosal axons through EphA3 signaling. *Journal of Neuroscience* **31**, 16251-16260 (2011).
78. Jung, R.E. & Haier, R.J. The Parieto-Frontal Integration Theory (P-FIT) of intelligence: converging neuroimaging evidence. *Behavioral and Brain Sciences* **30**, 135 (2007).
79. Deary, I.J., Penke, L. & Johnson, W. The neuroscience of human intelligence differences. *Nature reviews neuroscience* **11**, 201-211 (2010).
80. Linnér, R.K. *et al.* Genome-wide association analyses of risk tolerance and risky behaviors in over 1 million individuals identify hundreds of loci and shared genetic influences. *Nature Genetics* **51**, 245-257 (2019).
81. Floden, D., Alexander, M.P., Kubu, C., Katz, D. & Stuss, D.T. Impulsivity and risk-taking behavior in focal frontal lobe lesions. *Neuropsychologia* **46**, 213-223 (2008).
82. Consortium, C.-D.G.o.t.P.G. Identification of risk loci with shared effects on five major psychiatric disorders: a genome-wide analysis. *The Lancet* **381**, 1371-1379 (2013).
83. de Leeuw, C.A., Mooij, J.M., Heskes, T. & Posthuma, D. MAGMA: generalized gene-set analysis of GWAS data. *PLoS Computational Biology* **11**, e1004219 (2015).
84. Lek, M. *et al.* Analysis of protein-coding genetic variation in 60,706 humans. *Nature* **536**, 285 (2016).
85. Walker, R.L. *et al.* Genetic Control of Expression and Splicing in Developing Human Brain Informs Disease Mechanisms. *Cell* **179**, 750-771. e22 (2019).

86. Zhang, B. & Horvath, S. A General Framework for Weighted Gene Co-Expression Network Analysis. *Statistical Applications in Genetics & Molecular Biology* **4**, 1-43 (2005).
87. Watanabe, K., Taskesen, E., Bochoven, A. & Posthuma, D. Functional mapping and annotation of genetic associations with FUMA. *Nature Communications* **8**, 1826 (2017).
88. Wang, Q. *et al.* A Bayesian framework that integrates multi-omics data and gene networks predicts risk genes from schizophrenia GWAS data. *Nature neuroscience* **22**, 691 (2019).
89. Finucane, H.K. *et al.* Partitioning heritability by functional annotation using genome-wide association summary statistics. *Nature genetics* **47**, 1228-1235 (2015).
90. Hauberg, M.E. *et al.* Common schizophrenia risk variants are enriched in open chromatin regions of human glutamatergic neurons. *Nature communications* **11**, 1-16 (2020).
91. Matoba, N. & Stein, J.L. From base pair to brain. *Nature Neuroscience* **24**, 619-621 (2021).
92. Hansson, O. Biomarkers for neurodegenerative diseases. *Nature Medicine* **27**, 954-963 (2021).
93. Cole, M.W., Bassett, D.S., Power, J.D., Braver, T.S. & Petersen, S.E. Intrinsic and task-evoked network architectures of the human brain. *Neuron* **83**, 238-251 (2014).
94. Tavor, I. *et al.* Task-free MRI predicts individual differences in brain activity during task performance. *Science* **352**, 216-220 (2016).
95. Gonzalez-Castillo, J. & Bandettini, P.A. Task-based dynamic functional connectivity: Recent findings and open questions. *Neuroimage* **180**, 526-533 (2018).
96. Gratton, C. *et al.* Functional brain networks are dominated by stable group and individual factors, not cognitive or daily variation. *Neuron* **98**, 439-452. e5 (2018).
97. Pervaiz, U., Vidaurre, D., Woolrich, M.W. & Smith, S.M. Optimising network modelling methods for fMRI. *Neuroimage* **211**, 116604 (2020).

98. Dosenbach, N.U. *et al.* Prediction of individual brain maturity using fMRI. *Science* **329**, 1358-1361 (2010).
99. Betzel, R.F. *et al.* Changes in structural and functional connectivity among resting-state networks across the human lifespan. *Neuroimage* **102**, 345-357 (2014).
100. Dickie, E.W. *et al.* Ciftify: A framework for surface-based analysis of legacy MR acquisitions. *Neuroimage* **197**, 818-826 (2019).
101. Rolls, E.T., Huang, C.-C., Lin, C.-P., Feng, J. & Joliot, M. Automated anatomical labelling atlas 3. *NeuroImage* **206**, 116189 (2020).
102. Bijsterbosch, J. *et al.* Investigations into within-and between-subject resting-state amplitude variations. *Neuroimage* **159**, 57-69 (2017).
103. Bycroft, C. *et al.* The UK Biobank resource with deep phenotyping and genomic data. *Nature* **562**, 203-209 (2018).
104. Jiang, L. *et al.* A resource-efficient tool for mixed model association analysis of large-scale data. *Nature genetics* **51**, 1749 (2019).
105. Purcell, S. *et al.* PLINK: a tool set for whole-genome association and population-based linkage analyses. *The American Journal of Human Genetics* **81**, 559-575 (2007).

METHODS

Imaging datasets. We used the raw resting and task fMRI data from the UKB and HCP studies. The UKB study had obtained ethics approval from the North West Multicentre Research Ethics Committee (approval number: 11/NW/0382). All experimental procedures in the HCP study were approved by the institutional review boards at Washington University (approval number: 201204036). The image acquisition and preprocessing procedures were detailed in the **Supplementary Note**. The UKB task fMRI study implemented the emotion processing task[34,35]. In this study, the time series were extracted from the whole scan of the task fMRI data (including blocks of both Shape and Face activations, Data-Category 106). Thus, all contrasts were analyzed together when we calculated the functional connectivity measurements in downstream analysis. We used a parcellation-based approach based on the Glasser360 atlas[1]. Briefly, for each subject, we projected the resting and task fMRI data onto the Glasser360 atlas and obtained the 360

× 360 functional connectivity matrices. The original Glasser360 atlas is a surface-based parcellation for the cerebral cortex[100] and it has been transformed to a volumetric atlas that is compatible with the UKB volume-based data (**Supplementary Note**). The 360 functional areas were grouped into 12 functional networks[37] (**Table S1**). To aid interpretation, the 360 functional areas were labelled using the automated anatomical labeling atlas[101]. We examined the spatial overlaps between the Glasser360 functional areas and the whole brain ICA-defined brain regions generated from the previous 25-dimension and 100-dimensions ICA analyses[28]. A pairwise overlapping relationship was established if > 5% voxels of the ICA region were also in the Glasser360 area. We found most of the ICA-defined brain regions overlapped with multiple Glasser360 areas (**Figs. 1B** and **S2**).

We mainly studied two sets of fMRI traits: area-level traits and network-level traits. Area-level traits were the 8,531 functional connectivity measurements among all area pairs within each of the 12 networks, which provided fine details on cerebral cortex functional organizations and enabled the comparison between intrinsic and extrinsic functional architectures. Network-level traits were expected to aggregate the major information from the area-level traits. Specifically, we input the large number of area-level functional connectivity traits and extracted their low-rank representations/phenotypes via a combined PCA and ICA[27] dimension reduction approach in a training-validation design[29]. The low-rank imaging phenotypes were linear combinations of area-level traits and were independent with each other. We used a training-validation design (across two sets of independent subjects) to optimize both the initial dimensionality in the PCA step and the final number of ICA components (with the reproducibility of ICA weight vectors > 0.9). Such feature extraction was performed separately for area-level traits within each network (12 networks in total) and two sets of area-level traits belonging to a pair of networks (66 network work pairs in total, 12 × 11/2). The top low-rank imaging phenotypes were extracted from each of the 12 “within-network” analyses and the 66 “between-networks” analyses, which were interpreted as the network-level functional connectivity traits. Additionally, we considered the mean amplitude of each network (12 networks in total), which was a measure of brain activity[102]. The network-level feature extraction was performed separately for resting and task fMRI. Together, there were

1,985 network-level traits, 1,066 of which were from resting fMRI and 919 from task fMRI. Detailed steps of our parcellation-based dimension reduction procedure can be found in the **Supplementary Note** and the overview of the procedure and study design can be found in **Figure S1**. Overall, the network-level amplitude traits described the average brain activity across all brain functional areas within the network; and the network-level functional connectivity traits quantified the strength of functional connectivity within each network or between two different networks.

We analyzed the following datasets separately: 1) the white British discovery GWAS, which used data of individuals of white British ancestry in UKB phases 1 to 3 data (*n* = 34,641 for resting and 32,144 for task, released up through 2020); 2) European validation GWAS: UKB white but Non-British individuals in phases 1 to 3 data and all White individuals in newly released UKB phase 4 data (UKBW, *n* = 4,882 for resting and 4,023 for task); 3) two non-European UKB validation GWAS: UKB Asian (UKBA, *n* = 469 for resting and 368 for task) and UKB Black (UKBBL, *n* = 261 for resting and 191 for task); and 4) the UKB first revisit data (*n* = 1,491 for resting and 1,362 for task). The average age (at imaging) of all subjects was 64.16 (standard error = 7.73), 51.6% were females. The assignment of ancestry in UKB was based on self-reported ethnicity (Data-Field 21000), which was verified in Bycroft, et al. [103].

Heritability and GWAS analysis. We downloaded the imputed data from UKB data resources[103] (Data-Category 263). We performed the following quality controls on subjects with both imaging and genetics data: 1) excluded subjects with more than 10% missing genotypes; 2) excluded variants with minor allele frequency less than 0.01; 3) excluded variants with missing genotype rate larger than 10%; 4) excluded variants that failed the Hardy-Weinberg test at 1×10^{-7} level; and 5) removed variants with imputation INFO score less than 0.8. SNP heritability was estimated by GCTA[38] using all autosomal SNPs in the white British discovery GWAS. We adjusted the effects of age (at imaging), age-squared, sex, age-sex interaction, age-squared-sex interaction, imaging site, the top 40 genetic principal components (PCs)[103], as well as the head motion, head motion-squared, brain position, brain position-squared, and volumetric scaling. We also examined the genetic variance estimates from the GCTA. Genome-wide association

analysis was performed in linear mixed effect model using fastGWA[104], while adjusting the same set of covariates as in GCTA. GWAS were also separately performed via Plink[105] in validation datasets, where we adjusted for top ten genetic PCs instead of top 40. We removed values greater than five times the median absolute deviation from the median for each continuous phenotype or covariate variable. For area-level traits. the independent lead variants were clumped by Plink (LD $r^2 < 0.1$, --clump-r2 0.1 --clump-kb 250). The genomic loci associated with network-level traits were defined using FUMA[87] (version 1.3.5e). Specifically, to define the LD boundaries, FUMA identified independent significant variants, which were defined as variants with a *P*-value smaller than the predefined threshold and were independent of other significant variants (LD $r^2 < 0.6$). FUMA then constructed LD blocks for these independent significant variants by tagging all variants in LD ($r^2 \geq 0.6$) with at least one independent significant variant and had a MAF ≥ 0.0005. These variants included those from the 1000 Genomes reference panel that may not have been included in the GWAS. Moreover, within these significant variants, independent lead variants were identified as those that were independent from each other (LD $r^2 < 0.1$). If LD blocks of independent significant variants were close (<250 kb based on the closest boundary variants of LD blocks), they were merged into a single genomic locus. Thus, each genomic locus could contain multiple significant variants and lead variants. Independent significant variants and all the variants in LD with them ($r^2 \geq 0.6$) were searched on the NHGRI-EBI GWAS catalog (version 2019-09-24) to look for previously reported associations ($P < 9 \times 10^{-6}$) with any traits. We performed association analysis to illustrate association patterns for selected colocalized index variants across all 64,620 functional connectivity traits in resting and task fMRI. The significance threshold was set to be 3.86×10^{-7} (0.05/(64,620 × 2)). The same set of covariates used in the above GWAS analysis were adjusted in this analysis. LDSC[46] (version 1.0.1) was used to estimate and test genetic correlations. We used the pre-calculated LD scores provided by LDSC, which were computed using 1000 Genomes European data. We used HapMap3 variants and removed all variants in the major histocompatibility complex (MHC) region.

Gene-level analysis and biological annotation. Gene-based association analysis was performed in UKB white British discovery GWAS for 18,796 protein-coding genes using MAGMA[83] (version 1.08). Default MAGMA settings were used with zero window size

around each gene. We then carried out FUMA functional annotation and mapping analysis, in which variants were annotated with their biological functionality and then were linked to 35,808 candidate genes by a combination of positional, eQTL, and 3D chromatin interaction mappings. Brain-related tissues/cells were selected in all options and the default values were used for all other parameters in FUMA. For the 241 detected genes in MAGMA and FUMA, we performed lookups in the NHGRI-EBI GWAS catalog (version 2020-02-08) to explore their previously reported gene-trait associations. We also explored the overlaps with drug target genes using a nervous system drug target database[88], which contained 241 target genes for 273 nervous system drugs. We tested for whether the number of overlapping genes was greater than the expected number by chance using the Chi-squared test with resampling-based p-value. We performed heritability enrichment analysis via partitioned LDSC[89]. Baseline models were adjusted when estimating and testing the enrichment scores for our brain cell type specific annotations.

Code availability

We made use of publicly available software and tools. The codes used in fMRI preprocessing and the parcellation-based network level feature extraction pipeline will be shared on Zenodo.

Data availability

Our GWAS summary statistics will be shared on Zenodo and at BIG-KP https://bigkp.org/. The individual-level data used in the present study can be applied from the UK Biobank (https://www.ukbiobank.ac.uk/) and HCP (https://www.humanconnectome.org/).

Fig. 1 Illustration of the parcellation-based brain areas in the Glasser360 atlas and the comparison with selected whole brain ICA-defined brain regions.

(A) We illustrate the 360 functional areas and 12 networks defined in the Glasser360 atlas. In this paper, we generated functional connectivity traits based on these brain areas in both resting and task fMRI, providing area- and network-specific information about the genetic influences on the human brain functional originations. See Table S1 for

information of these Glasser360 areas. Visual1, the primary visual network; Visual2, the secondary visual network. **(B)** We illustrate the spatial overlaps between the functional areas defined in the Glasser360 atlas and two selected the whole brain ICA-defined brain regions (Net100_Node5 and Net100_Node44 in the left and right panels, respectively). The two ICA regions were previously generated from a 100-dimensions ICA analysis[28] (https://www.fmrib.ox.ac.uk/ukbiobank/) and were estimated to have a high level of heritability[30]. Here we show that the two ICA regions distribute across multiple brain areas and networks in the Glasser360 atlas (areas highlighted by dots with names being labelled). Specifically, the Net100_Node5 region (mainly in the precuneus, angular, middle cingulate) overlapped with 20 areas in the default mode, frontoparietal, and language networks, and the Net100_Node44 region (mainly in the inferior frontal) overlapped with 21 areas in the frontoparietal, language, cingulo-opercular, and default mode networks. A summary of such overlaps and more examples of ICA regions can be found in Figure S2.

Fig. 2 SNP heritability pattern in resting and task fMRI.

(A) The dots represent the SNP heritability estimates of fMRI traits, including 8,531 area-level and 1,066 network-level traits in resting fMRI (left panel), and 8,531 area-level traits and 919 network-level traits in task fMRI (right panel). The dots of non-significant heritability estimates (after controlling the false discovery rate of multiple testing at 5% level) had gray color. We labeled the mean heritability of each group. For example, the mean heritability of traits in the auditory network was 14.5% in resting fMRI. **(B)** Significant SNP heritability estimates of the functional connectivity traits within the default mode network in resting fMRI (white dots are insignificant estimates). We grouped all brain areas of the default mode network into seven clusters, which were mainly organized by their physical locations (Fig. S7). OFC, orbitofrontal complex. The *x* and *y* axis represent the names of the brain areas. **(C)** Comparison of SNP heritability between the activated areas (within activation, defined by the Shapes activation in task fMRI) and the nonactivated areas (out activation) in resting fMRI (upper panel) and task fMRI (lower panel). More information about the Shapes activation is available in Alfaro-Almagro, et al. [28].

Fig. 3 The associated genomic regions of fMRI traits.

(A) Ideogram of 47 genomic regions influencing fMRI traits, including 32 regions identified by area-level traits ($P < 2.93 \times 10^{-12}$) and 15 more identified by network-level traits ($P < 2.51 \times 10^{-11}$). The colors represent the 12 networks (and their interactions, named Between networks). Each signal dot indicates that at least one of the fMRI traits (area- or network-level) of this network is associated with the genomic region. The name of genomic regions replicated at the Bonferroni significance level and nominal significance level were highlighted in red and brown labels, respectively. **(B)** Functional areas associated with the 19q13.32 genomic region ($P < 2.93 \times 10^{-12}$), most of which were in the secondary visual network. The colors of brain areas represent different networks, and the name of significant brain areas were highlighted in read labels.

Fig. 4 Genetic locus associated with both fMRI traits and Alzheimer's disease.

In the 19q13.32 region, the *APOE* ε4 locus (index variant rs429358) was associated with both Alzheimer's disease and functional connectivity measurements. In **(A)**, we illustrate the shared genetic influences for one functional connectivity trait of the default mode network (Default <-> Default) in resting fMRI. In **(B)**, we illustrate the shared genetic influences for one functional connectivity trait of the secondary visual network (Visual 2 <-> Visual 2) in task fMRI. In **(C)**, we illustrate the *P*-value of associations between the rs429358 and different neuroimaging traits, including functional connectivity traits in resting fMRI, functional connectivity traits in task fMRI, as well as structural traits (in gray color), including diffusion tensor imaging (DTI) traits from diffusion MRI and regional brain volumes from structural MRI. The strongest genetic effects were observed in the secondary visual network for both resting and task fMRI.

Fig. 5 Selected pairwise genetic correlations between fMRI traits and cognitive function and schizophrenia.

(A) We illustrate significant genetic correlations with cognitive function across different networks in resting fMRI at the FDR 5% level. These significant genetic correlations were

particularly related to the functional connectivity traits of a few areas, such as the right IFSa in the cingulo−opercular network. **(B)** We illustrate significant genetic correlations with schizophrenia across different networks in resting fMRI at the FDR 5% level. These significant genetic correlations were particularly related to the functional connectivity traits of a few areas, such as the left 47s in the default mode network and the right LIPv in the secondary visual network. **(C)** We illustrate significant genetic correlations with cognitive function across different networks in task fMRI at the FDR 5% level. These significant genetic correlations were particularly related to the functional connectivity traits of a few areas, such as the left POS1 in the default mode network and the right V6 in the secondary visual network. Similar to the resting fMRI results in (A), genetic correlations with the default mode and dorsal attention networks were negative in task fMRI. However, the genetic correlations with the cingulo−opercular network became positive, and the somatomotor and secondary visual networks also had positive genetic correlations in task fMRI.

Fig. 6 Partitioned heritability enrichment analysis.

(A) Heritability enrichment of global functional connectivity and global amplitude of resting fMRI in regulatory elements of glial cells (glia, including all glial cells, oligodendrocyte subtype, and microglia/astrocyte subtype) and neuronal cells (neurons, including all neurons, GABAergic subtype, and glutamatergic subtype). The dashed lines indicate the nominal significance level. **(B)** Heritability enrichment of mean amplitude of the 12 functional networks in regulatory elements of glial and neuronal cell types.

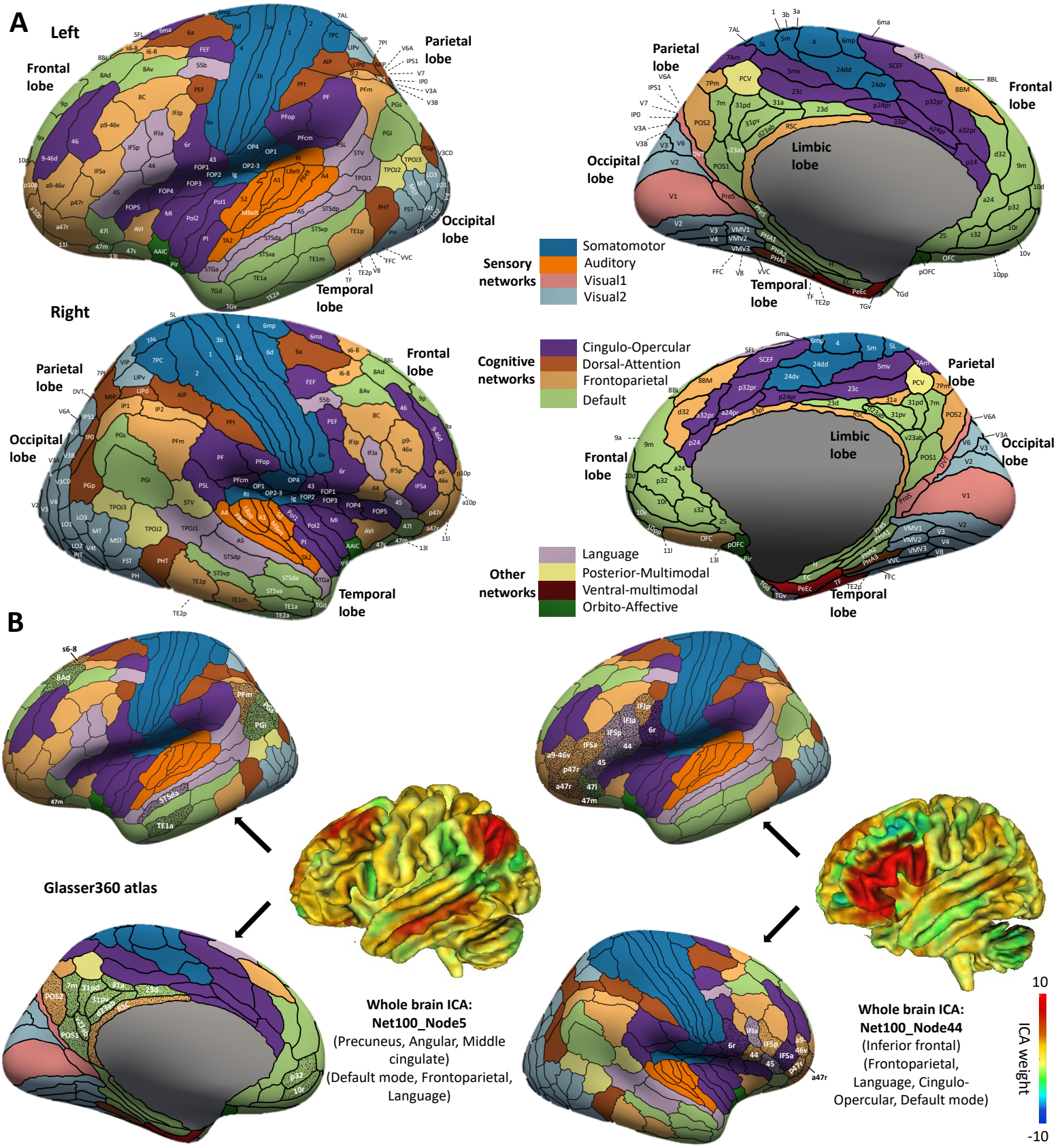
A
Left
Right
Frontal lobe
Parietal lobe
Occipital lobe
Temporal lobe
Limbic lobe
Sensory networks
Somatomotor
Auditory
Visual1
Visual2
Cognitive networks
Cingulo-Opercular
Dorsal-Attention
Frontoparietal
Default
Other networks
Language
Posterior-Multimodal
Ventral-multimodal
Orbito-Affective
B
Glasser360 atlas
Whole brain ICA:
Net100_Node5
(Precuneus, Angular, Middle cingulate)
(Default mode, Frontoparietal, Language)
Whole brain ICA:
Net100_Node44
(Inferior frontal)
(Frontoparietal, Language, Cingulo-Opercular, Default mode)
10
ICA weight
-10

Figure 1

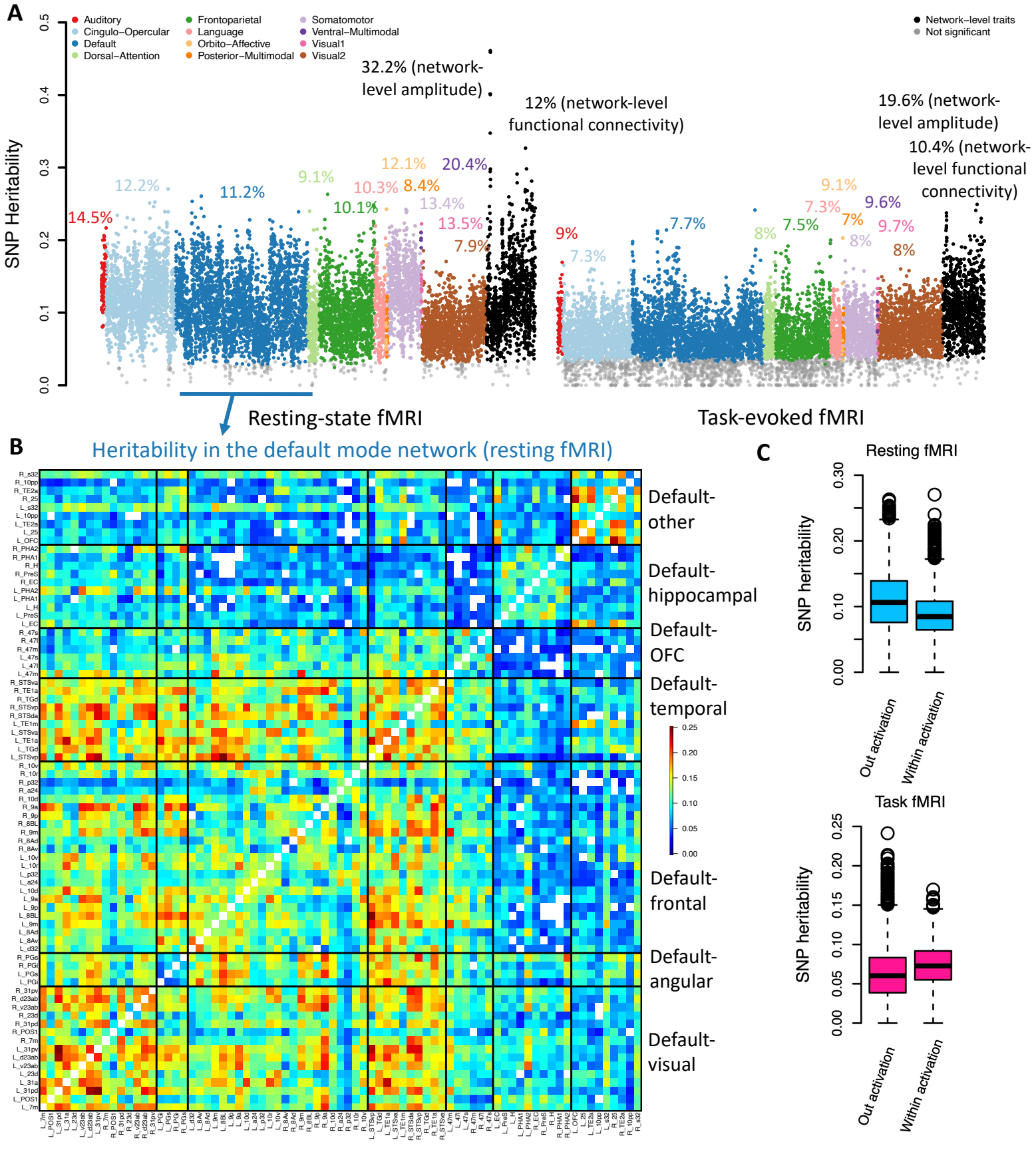
A
Auditory
Cingulo−Opercular
Default
Dorsal−Attention
Frontoparietal
Language
Orbito−Affective
Posterior−Multimodal
Somatomotor
Ventral−Multimodal
Visual1
Visual2
Network−level traits
Not significant
SNP Heritability
32.2% (network-level amplitude)
12% (network-level functional connectivity)
19.6% (network-level amplitude)
10.4% (network-level functional connectivity)
14.5%
12.2%
11.2%
9.1%
10.1%
12.1%
10.3%
8.4%
20.4%
13.4%
13.5%
7.9%
9%
7.3%
7.7%
8%
7.5%
9.1%
7.3%
7%
8%
9.6%
9.7%
8%
Resting-state fMRI
Task-evoked fMRI
B
Heritability in the default mode network (resting fMRI)
Default-other
Default-hippocampal
Default-OFC
Default-temporal
Default-frontal
Default-angular
Default-visual
C
Resting fMRI
SNP heritability
Out activation
Within activation
Task fMRI
SNP heritability
Out activation
Within activation

Figure 2

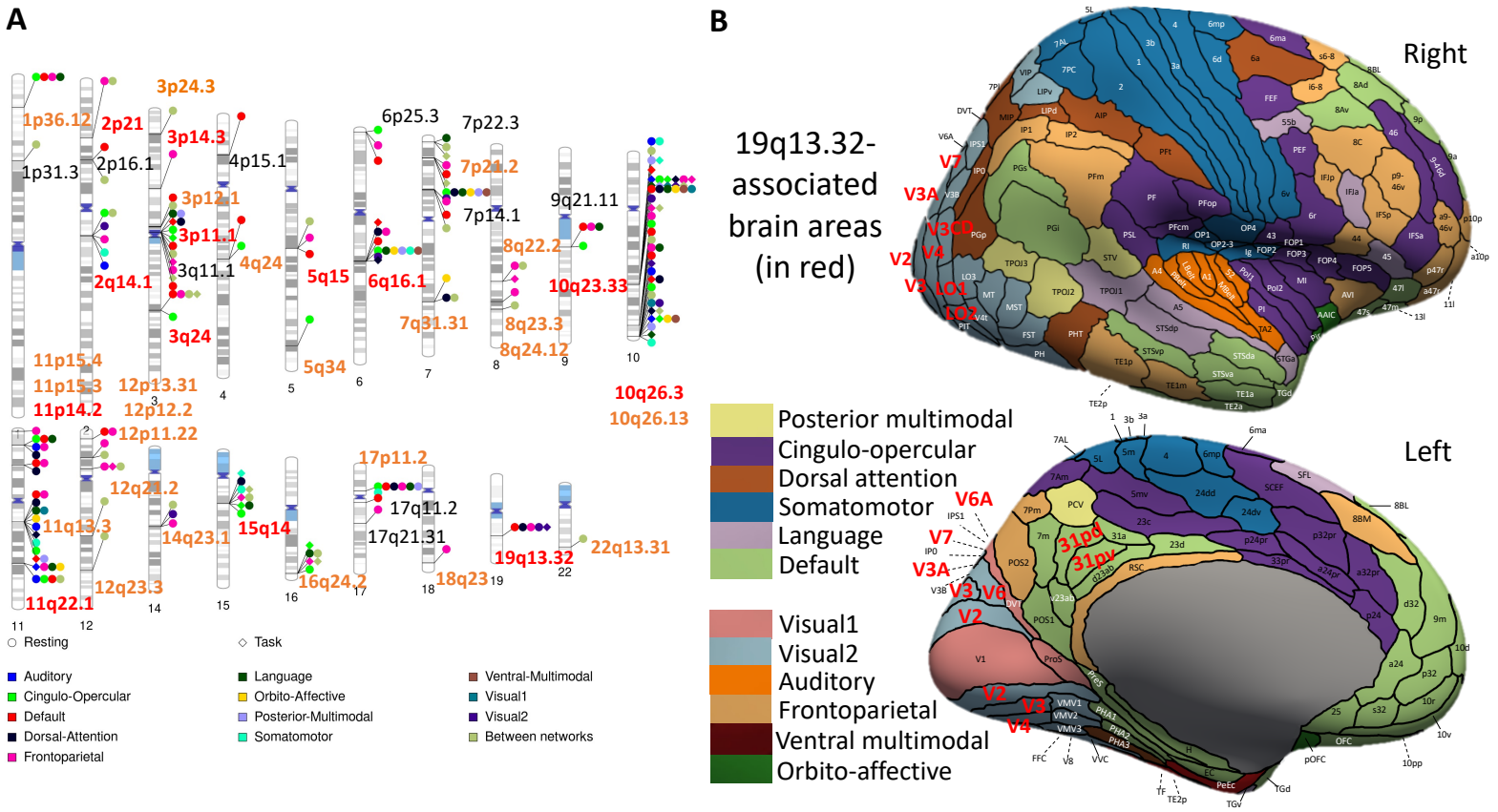
A
B
1p36.12
2p21
3p24.3
3p14.3
1p31.3
2p16.1
4p15.1
3p12.1
3p11.1
3q11.1
4q24
2q14.1
5q15
6p25.3
6q16.1
7p22.3
7p24.2
7p14.1
7q31.31
9q21.11
8q22.2
8q23.3
8q24.12
10q23.33
3q24
5q34
11p15.4
11p15.3
11p14.2
12p13.31
12p12.2
10q26.3
10q26.13
12p11.22
12q21.2
11q13.3
14q23.1
15q14
17p11.2
17q11.2
17q21.31
19q13.32
22q13.31
18q23
16q24.2
12q23.3
11q22.1
Resting
Task
Auditory
Cingulo-Opercular
Default
Dorsal-Attention
Frontoparietal
Language
Orbito-Affective
Posterior-Multimodal
Somatomotor
Ventral-Multimodal
Visual1
Visual2
Between networks
19q13.32-associated brain areas (in red)
Right
Left
V7
V3A
V3CD
V2
V4
V3
LO1
LO2
V6A
V6
31pd
31pv
Posterior multimodal
Cingulo-opercular
Dorsal attention
Somatomotor
Language
Default
Visual1
Visual2
Auditory
Frontoparietal
Ventral multimodal
Orbito-affective

Figure 3

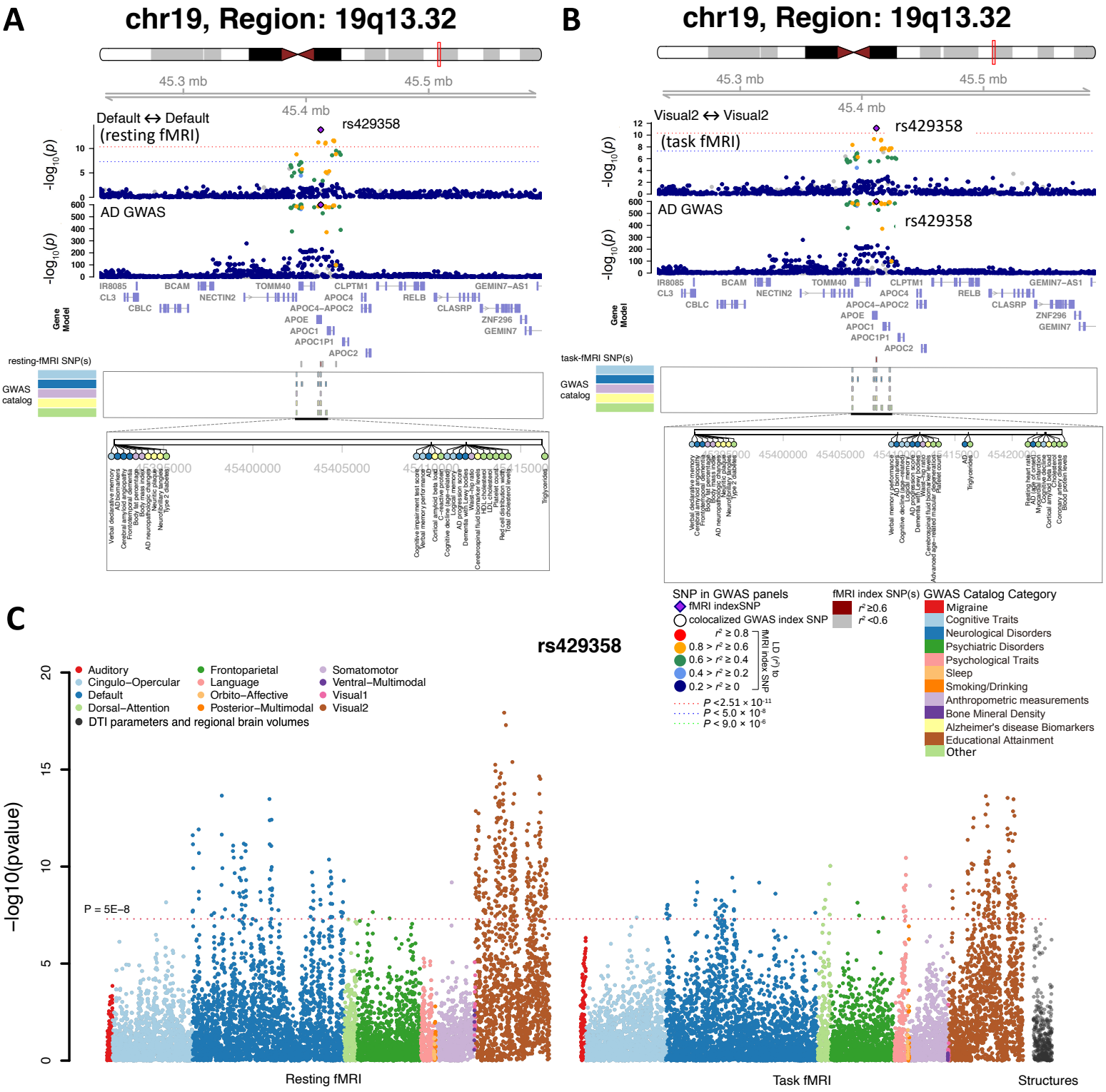
A
chr19, Region: 19q13.32
45.3 mb
45.5 mb
45.4 mb
Default ↔ Default
(resting fMRI)
rs429358
-log10(p)
AD GWAS
Gene Model
resting-fMRI SNP(s)
GWAS catalog
B
chr19, Region: 19q13.32
Visual2 ↔ Visual2
(task fMRI)
task-fMRI SNP(s)
SNP in GWAS panels
fMRI indexSNP
colocalized GWAS index SNP
LD (r²) to fMRI index SNP
fMRI index SNP(s)
GWAS Catalog Category
Migraine
Cognitive Traits
Neurological Disorders
Psychiatric Disorders
Psychological Traits
Sleep
Smoking/Drinking
Anthropometric measurements
Bone Mineral Density
Alzheimer's disease Biomarkers
Educational Attainment
Other
C
rs429358
Auditory
Cingulo−Opercular
Default
Dorsal−Attention
Frontoparietal
Language
Orbito−Affective
Posterior−Multimodal
Somatomotor
Ventral−Multimodal
Visual1
Visual2
DTI parameters and regional brain volumes
−log10(pvalue)
P = 5E−8
Resting fMRI
Task fMRI
Structures

Figure 4

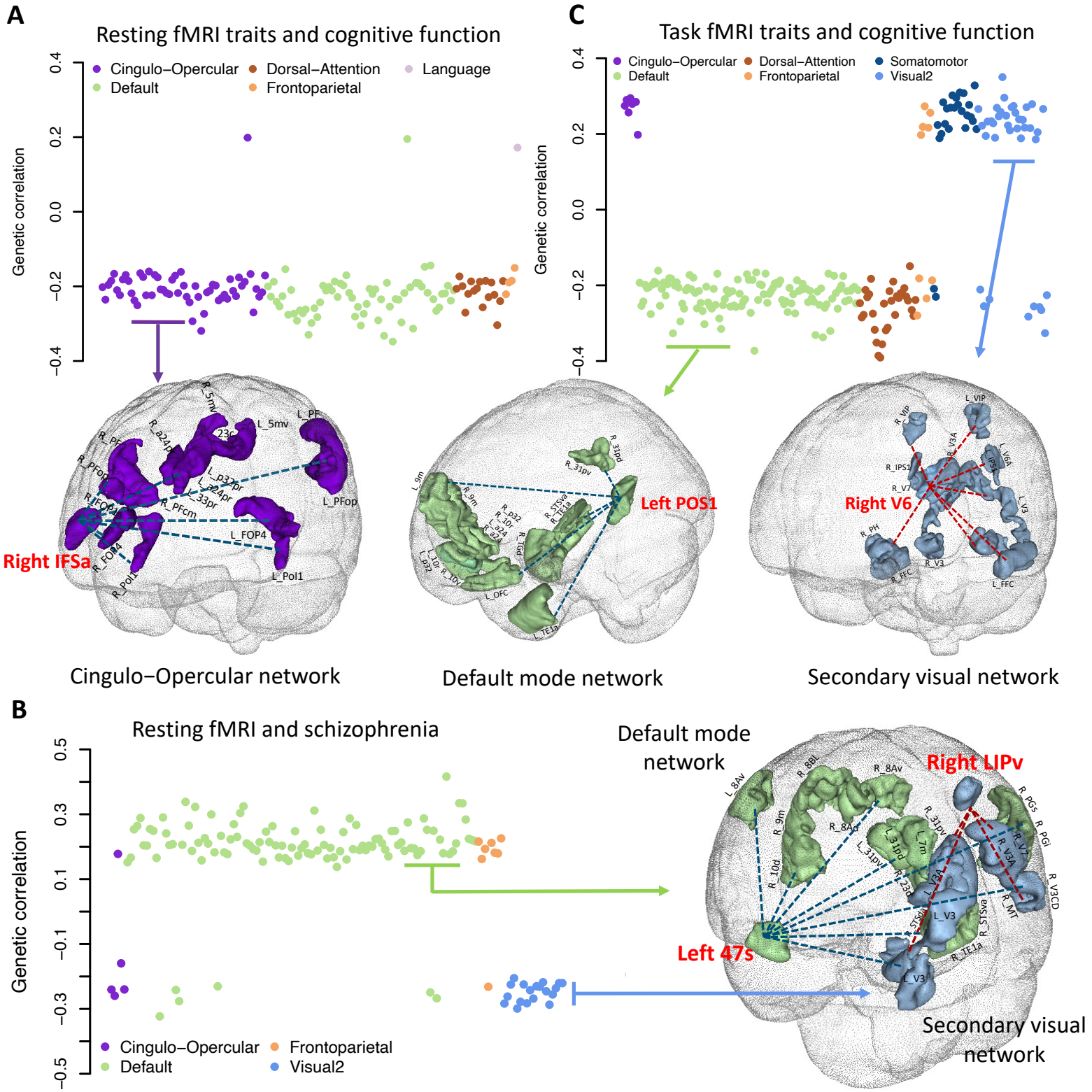
A
Resting fMRI traits and cognitive function
Cingulo−Opercular
Dorsal−Attention
Language
Default
Frontoparietal
Genetic correlation
0.4
0.2
0.0
−0.2
−0.4
Right IFSa
Cingulo−Opercular network
C
Task fMRI traits and cognitive function
Cingulo−Opercular
Dorsal−Attention
Somatomotor
Default
Frontoparietal
Visual2
Genetic correlation
Left POS1
Default mode network
Right V6
Secondary visual network
B
Resting fMRI and schizophrenia
Genetic correlation
0.5
0.3
0.1
−0.1
−0.3
−0.5
Cingulo−Opercular
Frontoparietal
Default
Visual2
Default mode network
Right LIPv
Left 47s
Secondary visual network

Figure 5

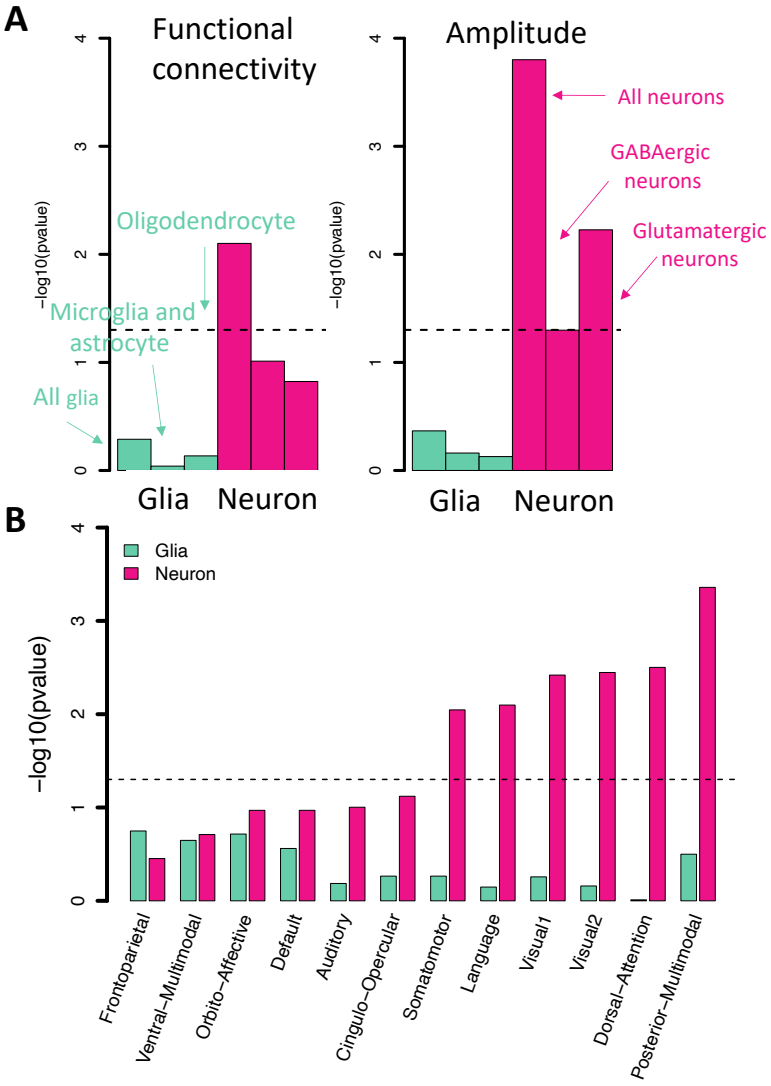
A
Functional connectivity
Amplitude
−log10(pvalue)
Oligodendrocyte
Microglia and astrocyte
All glia
All neurons
GABAergic neurons
Glutamatergic neurons
Glia
Neuron
B
Glia
Neuron
−log10(pvalue)
Frontoparietal
Ventral−Multimodal
Orbito−Affective
Default
Auditory
Cingulo−Opercular
Somatomotor
Language
Visual1
Visual2
Dorsal−Attention
Posterior−Multimodal

Figure 6